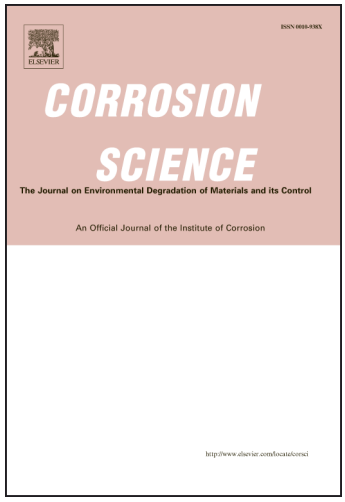

Kinetics and Mechanism of Isothermal Oxidation of Compositionally Graded Yttria Stabilized Zirconia (YSZ) based Thermal Barrier Coating

Subhasisa Nath, Indranil Manna, Jyotsna Dutta Majumdar

PII: S0010-938X(14)00316-3
DOI: http://dx.doi.org/10.1016/j.corsci.2014.06.050
Reference: CS 5921

To appear in: *Corrosion Science*

Received Date: 10 April 2014
Accepted Date: 30 June 2014

Please cite this article as: S. Nath, I. Manna, J.D. Majumdar, Kinetics and Mechanism of Isothermal Oxidation of Compositionally Graded Yttria Stabilized Zirconia (YSZ) based Thermal Barrier Coating, *Corrosion Science* (2014), doi: http://dx.doi.org/10.1016/j.corsci.2014.06.050

Kinetics and Mechanism of Isothermal Oxidation of Compositionally Graded Yttria Stabilized Zirconia (YSZ) based Thermal Barrier Coating

Subhasisa Nath[a1], Indranil Manna[a,b2], Jyotsna Dutta Majumdar[a, 3*]

[a]Department of Metallurgical and Materials Engineering, Indian Institute of Technology, Kharagpur 721302, West Bengal, India
[b]Indian Institute of Technology, Kanpur 208016, Uttar Pradesh, India
[1]: sendsubha@gmail.com; [2]:imanna@metal.iitkgp.ernet.in; [3]:jyotsna@metal.iitkgp.ernet.in

Abstract

The present study concerns studying the isothermal oxidation behavior of compositionally graded thermal barrier coating (TBC) consisting of 100% CoNiCrAlY as bond coat developed by high velocity oxyfuel (HVOF) spraying on Inconel 718 substrate followed by several layers of CoNiCrAlY and YSZ in the weight ratios of 70:30, 50:50, 30:70, and 0:100 by plasma spraying. The kinetics of growth of the thermally grown oxide (TGO) layer developed due to oxidation of compositionally graded TBC was compared to the same grown during oxidation of conventional duplex TBC. The mechanism of oxidation was established. The residual stress developed on the surface before and after oxidation was studied in details.

Keywords: A. Ceramic; A. Superalloys; B. XRD; B. SEM; C. Oxidation

*Corresponding author, FAX: +91-3222-282280

1. Introduction

Thermal barrier coating (TBC) consists of a low thermal conductivity yttria stabilized zirconia (YSZ) ceramic top coat and a metallic bond coat of MCrAlY type (where M= Co, Ni, or both) deposited on superalloy substrate to protect the gas turbine engine components such as combustors, blades, and vanes from high temperature degradation [1]. TBC system usually fails due to (a) thermal expansion mismatch between the ceramic top coat and metallic bond coat and (b) growth of thermally grown oxide (TGO) layer formed on the surface of bond coat during service [2,3]. The residual stress developed at the interface between top coat and bond coat may be minimized by application of a functionally graded coating achieved by the continuous variation of composition throughout the coating thickness eliminating sharp interface between two successive coating layers [4-7]. Khor *et al*. [8-11] used pre-alloyed composite powders to deposit functionally graded TBC without any sharp interface between successive layers, leading to a gradual variation of mechanical and thermal properties across the coating thickness, and thereby, improving the coating life. The bond strength and thermal cyclic resistance of the TBC was reported to be improved as a result of compositional gradation [12]. The growth of TGO during service on the bond coat alloy induces growth stress (< 1 GPa) and thermal expansion mismatch stress between the bond coat alloy and TGO and TGO and top coat which limits the component life [13]. Thus, lowering the TGO growth rate could be advantageous in enhancing the component life. Many investigations were carried out to improve the bond coat oxidation resistance by modifying the conventional bond coat alloy [14, 15]. The oxidation resistance of the bond coat alloy also improved by providing a gradient bond coating as well as proving an NiAl inter layer or diffusion barrier layer [16-19]. Modifications in the coating deposition

processes have also been effective in improving the oxidation resistance of the TBC system [20, 21]. Efforts have also been made to replace the conventional bond coats by the application of laminated Al_2O_3-Y_2O_3/ YSZ laminated coating to improve the oxidation resistance as well as the mechanical properties of the TBC system [13, 22]. The compositionally graded interlayer also helped to improve the oxidation resistance by forming a protective Al_2O_3 scales in the graded layers, whose growth rate is slower that the conventional TBC [9]. Chemical composition of TGO also plays a crucial role in the failure of TBC. Al_2O_3 as TGO is preferable due to its dense microstructure, better adherence to the bond coat, and barrier to oxygen transport. In this regard, it is relevant to mention that even though a large numbers of studies have been undertaken on the oxidation behavior of YSZ based thermal barrier coating, only a few literatures concern the detailed investigation of the kinetics and mechanism of oxidation based on growth of TGO.

Plasma spraying is a deposition process where, a high temperature plasma plume (>10000 K) is used for melting of powders and subsequently, the molten or semi-molten material is accelerated by high velocity gas towards the substrate to form coating [23, 24]. Presence of microcracks, and porosities in the microstructure of plasma sprayed ceramic top coating is beneficial in reducing the thermal conductivity of coating and increasing its strain tolerance during exposure to thermal cycling. It has been observed that a dense YSZ coating with high modulus (E= 200 GPa) when cooled from high temperature to ambient develops a large residual thermal stress than a plasma sprayed coating with low modulus (E= 50 GPa) [25]. Furthermore, the oxidation resistance property of plasma sprayed surface is inferior due to the presence of defects in the microstructure. However, the bond coat used for thermal spray deposition should offer a significant improvement in oxidation resistance property, which demands the presence of dense and pore free microstructure. High velocity oxy-fuel (HVOF) spraying is a technique for

the development of dense coating (with 99% density) which utilizes heat generated by combustion of oxygen and fuel to heat powder to its semi-molten/molten state and subsequently, deposited on the surface of the substrate at a velocity higher than sonic velocity [26, 27]. In the past, HVOF spraying has been successfully applied for the deposition of nano-boride dispersed coating on AISI 304 stainless steel and copper substrates with improved wear and corrosion resistance [28,29]. In an earlier attempt, the detailed characterization and non-isothermal oxidation behavior of compositionally graded CoNiCrAlY/YSZ thermal barrier coatings developed by hybrid deposition route has been studied and it was observed that compositionally graded thermal barrier coating showed superior oxidation behavior as compared to the duplex coating [30]. However, detailed studies on the isothermal oxidation behavior and the effect of oxidation on the scale properties have not been undertaken which is important for the possibility of its application in power generation.

In the present study, a detailed investigation of the isothermal oxidation behavior (kinetics and mechanism) of compositionally graded YSZ/CoNiCrAlY TBC developed on Inconel 718 substrate has been undertaken and compared with the duplex coated substrate. Compositionally graded coating consisted of several layers of coatings with 100% CoNiCrAlY as bond coat developed by HVOF spraying on Inconel 718 substrate followed by several layers of CoNiCrAlY and YSZ in the weight ratios of 70:30 (of thickness 80 μm on the bond coat as the first intermediate layer), 50:50 (of thickness 80 μm as the second intermediate layer), 30:70 (of thickness 80 μm as the third intermediate layer), and 0:100 (of thickness 100 μm as the top layer) developed by plasma spray deposition technique. On the other hand, duplex coating consists of 100% YSZ top coating (developed by plasma spray deposition) on the top of 100% CoNiCrAlY

bond coat (developed by HVOF spray deposition). The effect of isothermal exposure on residual stress state of coating layers was also studied.

2. Experimental

Ni-based superalloy (Inconel 718 with nominal compositions: Ni-18.8Fe-14Cr-7.3Nb-1.7Mo-1.3Ti-0.7Al in wt.%) of 20 mm × 20 mm × 5 mm dimensions were used as substrate. CoNiCrAlY bond coat (Co-32Ni-21Cr-8Al-0.5Y in wt.%) was deposited on sand blasted Inconel 718 superalloy substrate using high velocity oxy-fuel spray (HVOF) technique. For the development of duplex thermal barrier coating (TBC), 7 wt% yttria stabilized zirconia (YSZ) powder (15-85 μm) was sprayed on the bond coated surface by atmospheric plasma spray technique (APS) using a 80 kW plasma torch (SG 100, Miller Thermal Inc. USA). For the development of compositionally graded thermal barrier coating, a mixtures of CoNiCrAlY and 7YSZ powders in the weight ratio of 70:30 (of thickness 80 μm on the bond coat as the first intermediate layer), 50:50 (of thickness 80 μm as the second intermediate layer), 30:70 (of thickness 80 μm as the third intermediate layer), and 0:100 (of thickness 100 μm as the top layer) were deposited sequentially in a layer by layer fashion by atmospheric plasma spray technique (APS) on HVOF spray deposited CoNiCrAlY coating.

Isothermal oxidation studies of the coated and uncoated samples were undertaken by holding the diamond polished coated surface isothermally in air at temperatures ranging from 900 °C to 1000 °C and subsequently, measuring the weight change and the thickness of thermally grown oxide (TGO) layer at an interval of 24 hours up to a maximum of 96 hours. Thirty measurements were averaged out to calculate the TGO thickness. Followed by isothermal

oxidation, a detailed observation of the microstructure of the oxide scale was undertaken by scanning electron microscopy (SUPRA 40, Zeiss SMT AG, Germany). A detailed analysis of the phase and composition was carried out by the x-ray diffraction (XRD) technique (D8 Advances, Bruker AXS, Germany) and energy dispersive X-ray spectroscopy (EDS), respectively. Residual stress (both micro and macro) developed on the surface was carefully measured by XRD analysis using a stress Goniometer for macro-stress (PW 3040/60, Panalytical X'pert Pro, Netherland) and peak broadening analysis using Scherrer's formula for micro-stress [31].

3. Results and Discussion

3.1. As-sprayed microstructural analysis

Fig. 1 shows the scanning electron micrographs of the (a) cross-section of the duplex thermal barrier coating developed by plasma spray deposition technique, (b) high magnification view of the same, (c) cross-section of high velocity oxy-fuel spray deposited CoNiCrAlY bond coat and the same at (d) high magnification. Fig. 1a shows the presence of voids and porosities heterogeneously distributed throughout the coating thickness of the top coat. Mechanical interlocking of the ceramic top with metallic bond coat can be seen at the interface between the top coat and bond coat. The high magnification view of Fig. 1a (cf. Fig. 1b) shows the presence of micro-porosities (labeled as 1), inter-lamellar pores (labeled as 2), intra-lamellar cracks (labeled as 3) and inter-lamellar cracks (labeled as 4). Improper melting and solidification of in-flight powder particles and entrapment of carrier gas result in the formation of voids and porosities [14]. Porosity content is found to vary from 8 to 14% in duplex thermal barrier coating. Intra-lamellar cracks were formed due to the stress relaxation during rapid solidification of the individual splats [24]. The presence of inter-lamellar porosities and inter-lamellar cracks

were due to poor bonding between consecutive splats. It has been observed that presence of the micro-cracks, and porosities makes the ceramic coating more strain tolerant by accommodating stress during thermal cycling [32, 33]. Presence of horizontally oriented cracks/porosities is thought to have detrimental effect on coating integrity as they act as the source of delamination [34]. However, they help to minimize the thermal conductivity of the coating by providing active sites for phonon scattering[32-34]. Fig. 1c shows the microstructure of the cross-section of the bond coat revealing its dense nature. The light grey phase in Fig. 1d is the γ/γ' matrix and dark grey phase is β-CoAl. The γ/γ' and β phases are differentiated in terms of their aluminium concentration. The concentration of aluminium in β phase (with composition: 16.82 at. % Co, 44.12 at. % Ni, 6.46 at. % Cr, and 32.6 at. % Al) is higher than γ/γ' phase (with composition: 38 at. % Co, 28.35 at. % Ni, 26.78 at. % Cr, and 6.86 at. % Al) as observed from EDS analysis. The β phase acts as an aluminium reservoir in CoNiCrAlY coating which supplies aluminium towards the bond coat surface or bond coat and top coat interface in TBC during oxidation to form stable Al_2O_3 [35]. The presence of γ/γ' and β phases are also confirmed by X-ray diffraction study (cf. Fig. 9, plot 1). The area fraction of porosities and microcracks is negligible in HVOF spray deposited coating.

Fig. 2 represents the scanning electron micrographs (in back scattered mode) of (a) cross-section of as-sprayed compositionally graded thermal barrier coating and the different regions of the same at high magnification showing (b) top 100% YSZ layer (zone 1), (c) 70% YSZ+30% CoNiCrAlY (zone 2), (d) 50% YSZ+50% CoNiCrAlY (zone 3), and (e) 30% YSZ+70% CoNiCrAlY (zone 4). From Fig. 2a, it can be seen that the gradual variation in composition through the coating thickness, eliminates the formation of sharp interface between coating layers

which has also a beneficial effect in reducing the residual thermal stress in the coating [4-7]. The porosity content in the graded coating is found to vary between 7 to 10 %. The presence of porosities is beneficial in terms of enhancing the coating life by making it strain tolerant [32, 33]. The porosity distribution is not uniform throughout the coating thickness, which is attributed to the difference in the size of CoNiCrAlY powder and the YSZ powder particles and also difference in the density of CoNiCrAlY and YSZ powders. The formation of porosities in the coating depends on the deposition parameters [33]. But in the present study, we have maintained a set of constant parameters for the development of duplex as well as graded thermal barrier coating. From Fig. 2b, it can be seen that the 100% YSZ coating layers contains micro features such as cracks, porosity which are oriented both in horizontal as well as vertical direction (as observed in Fig. 1b). From Fig. 2c to e, it can be seen that the micro-cracks and inter-lamellar porosities varies with the volume fraction of CoNiCrAlY present in the graded layers. Presence of microcracks and porosities are maximum in 100% YSZ layer and reduces with depth in the subsequent layers which is due to stress relaxation by individual splats and poor bonding between splats. Only vertically oriented intra-splat cracks are found to be present in the 30% YSZ + 70% CoNiCrAlY layer due to quenching stress relaxation by the splat after solidification. The area fraction of inter-lamellar porosities in the 4^{th} layer (30% YSZ + 70% CoNiCrAlY) is significantly reduced which indicates a good bonding between splats of YSZ and CoNiCrAlY. The decrease in the porosity content in graded layer near to bond coat helps to improve the mechanical integrity of TBC. The different phases present in Fig. 2 are labeled as A-D. A detailed energy dispersive x-ray spectroscopic analysis was undertaken to determine the phases present in the different zones as labeled and are summarized in Table 1. From Table 1, it may be concluded that region A is predominantly YSZ, region B is CoNiCrAlY bond coat, region C is

Al_2O_3 and region D is the oxides of Co, Ni, Cr and Al (spinel in nature), which is formed during plasma spraying due to oxidation of Al, Cr, Ni, Co present in the bond coat. The area fraction of oxide phase increased with increase in the volume fraction of CoNiCrAlY in the graded layers. It can be seen that the coating is having splat like appearance which is the characteristic of plasma spraying.

3.2. ***Growth kinetics of thermally grown oxide layer***

Oxidation of bond coat occurs due to the diffusion of atmospheric oxygen through the porous zirconia coating. The mechanism of diffusion through the top coat are; (i) ionic movement of oxygen, and (ii) oxygen ingress through interconnected pores and cracks [38]. Isothermal oxidation experiments were conducted on duplex thermal barrier coating, compositionally graded thermal barrier coating, and bond coated samples at 900 °C, 950 °C, and 1000 °C to evaluate the kinetics and mechanism of oxidation. Fig. 3 shows the variation in thickness of thermally grown oxide layer (TGO) with time during isothermal exposure at (a) 900 °C, (b) 950 °C, and (c) 1000 °C in air. In all the three reference temperatures, the kinetics of growth of TGO is very fast in the transient stage which approaches a steady state beyond a certain period of time. The initial higher kinetics of TGO formation is attributed to availability of aluminium and formation of Al_2O_3 scale (due to its lowest free energy of formation). However, the slower kinetics of diffusion at a later stage is attributed to the coverage of the surface with Al_2O_3 which acts as a diffusion barrier, offering resistance to further oxygen diffusion and approaching towards steady state [4, 9, 39, 40]. The variation of TGO thickness with time is found to follow parabolic law after the transient stage. The TGO growth kinetics can be expressed through a typical equation [36, 37].

$$x^n = k_p t \quad (1)$$

where, x is the thermally grown oxide layer thickness (μm) , t is the time (h), the value of exponent (n) is taken as 2 (assuming diffusion assisted the growth mechanism) and k_p is the rate constant.

From Fig. 3 it can be seen that the thickness and kinetics of TGO layer is higher in duplex coating than that of compositionally graded thermal barrier coatings at all three temperatures of oxidation. From Fig 3a, it can be noted that the difference in TGO growth rate of duplex and graded TBC is maximum at 900 °C. However, with increase in oxidation temperature the difference in TGO growth rate in duplex and graded TBC reduces due to increased kinetics of diffusion at higher temperature as observed from Fig. 3b and c. In an earlier study, during non-isothermal oxidation similar behavior was observed [30]. A detailed study on the mechanism of non-isothermal oxidation showed that in duplex TBC, the protective oxide scale forms at the bond coat-top coat interface. On the other hand, in graded TBC, the oxide layers were found to form all throughout the coating in an intermittent manner, protecting the surface as a diffusion barrier and also closing the pores/cracks by the oxide scale [30]. This in turn creates a partial pressure drop at the bond coat-top coat interface in the case of compositionally graded TBC as compared to duplex TBC. A reduced supply of oxygen at the bond coat-top coat interface leads to a reduced oxidation in compositionally graded coating as compared to duplex TBC. These effects contribute to the lower growth rate of TGO in compositionally graded TBC.

Figs. 4a and b show the variation of square of thermally grown oxide layer thickness with time of isothermal exposure for duplex and graded thermal barrier coatings, respectively. From the slope of kinetics plots in Fig. 4, the rate constants for the growth of TGO (for both the duplex

and graded TBC) were calculated and are summarized in Table 2. From Table 2, it may be noted that k_p for graded coating is lower than the duplex one. The lower rate constant of the graded coating is attributed to a reduced rate of oxidation in graded coating as compared to the duplex one.

Fig. 5 shows the Arrhenius plot showing the variation of parabolic rate constant (ln k_p) as a function of inverse of temperature (T). The Arrhenius parameters are summarized in Table 2. From Table 2, it may be noted that the apparent activation energies of isothermal oxidation (in the temperature range between 900 °C to 1000 °C) of duplex and compositionally graded thermal barrier coatings are 129 kJ/mol and 175 kJ/mol, respectively. Hence, it may be concluded that graded thermal barrier coating offers a higher oxidation resistance under isothermal oxidation than the duplex coating.

In this regard, it is relevant to mention that the manufacturing cost for the development of a graded TBC is higher than that of duplex TBC, however, the graded TBC showed five times improvement in thermal cycling life than that of conventional duplex TBC [9], which justifies the applicability of the graded coating for thermal barrier application.

3.3. Post oxidation analysis

To understand the mechanism of oxidation, a detailed study of the top surface and cross section of the oxide scale were undertaken by scanning electron microscopy, x-ray diffraction technique and energy dispersive spectroscopic analysis.

3.3.1. Microstructural Investigation

Fig. 6 shows the scanning electron micrographs of the cross section of (a,c) duplex and (b,d) compositionally graded thermal barrier coating isothermally oxidized at 1000 °C for 96 hours at (a,b) low and (c,d) high magnification. From Fig. 6a, it may be noted that the thermally grown oxide (TGO) layer is formed at the interface of CoNiCrAlY bond coat and YSZ top coat. The oxides formed at the bond coat-top coat interface helps to protect the substrate from oxidation by acting as a diffusion barrier against oxygen. Fig. 6b shows the microstructure of the compositionally graded TBC after isothermal oxidation at 1000 °C for 96 hour. From the microstructure of oxidized compositionally graded TBC, it can be seen that oxide scales are distributed throughout the cross-section of the coating in an intermittent fashion instead of a monolithic oxide scale which is mainly composed of Al_2O_3 at the bond coat-top coat interface. The presence of discontinuous oxide scales present in the graded layers was reported to improve the oxidation resistance of graded thermal barrier coating [9]. From Fig. 6c, it can be seen that a thermally grown oxide (TGO) layer has been formed in a continuous manner at the interface of metallic CoNiCrAlY bond coat and ceramic YSZ top coat. The formation of TGO is due to reaction of elements present in the CoNiCrAlY bond coat with oxygen transported through the YSZ top coat at elevated temperature. Fig. 6d shows the formation of continuous TGO layer at the interface between CoNiCrAlY bond coat and graded top coat as well as the formation of oxide layer at the graded region in an intermittent fashion. During oxidation, oxygen initially diffuses through the interconnected porosities and microcracks present in the coating and by lattice diffusion as YSZ is good ionic conductor, and thereby oxidizing the bond coat forming

TGO at the bond coat-top coat interface. As graded layers contain metallic bond coat in different fractions they initially get oxidized along with pure bond coat. As soon as stable oxides form, they retard oxygen diffusion further towards bond coat-top coat interface and thereby decreasing the partial pressure of oxygen at the bond coat-top coat interface. Decrease in partial pressure of oxygen reduces the growth kinetics of TGO in graded TBC. From Fig. 6c, it is evident that TGO consists of bi-layers, a dark grey oxide layer labeled as (1) which was found to be Al_2O_3 (with composition of 36.02-38.37 at. % Al and 61.62-63.98 at. % O as determined by EDS analysis) and light grey oxide layer labeled as (2) which was found to be a mixed spinel oxides of Co, Ni, Cr, and Al (with composition: 5.58-6.59 at. % Co, 2.75-3.22 at. % Ni, 3.44-7.79 at. % Cr, 25.06-29.95 at. % Al and 57.80-57.81 at. % O as determined by EDS analysis). CoNiCrAlY bond coat contains approximately 8 wt% of aluminum and 21 wt% of chromium which upon exposure to high temperature oxidizing environment forms various oxides of Al_2O_3, Cr_2O_3, spinels etc. on top of bond coat. The composition of TGO plays an important role in determining the life time of TBC as the presence of spinels reduces the toughness of the interface containing TGO. In addition, the higher growth kinetics of spinel oxide is found to have a detrimental effect on the life of TBC [35, 45]. Hence, a complete understanding on the mechanism of oxide formation needs to be undertaken to assess the kinetics of TGO growth.

Figs. 7a and b show the scanning electron micrographs of the cross section of isothermally oxidized CoNiCrAlY bond coat at 1000 °C for 96 hrs and (b) high magnification view of the same. From Fig. 7a, it is evident that the oxide scale forms on top of the bond coat. The oxide scale was found to be composed alumina, chromia and spinel oxides. From Fig. 7b, it can be seen that two phase regions (γ-Co and β-CoAl) were observed in the oxidized cross-section of CoNiCrAlY bond coat samples. A close observation of Fig. 7b shows that the oxide

scale is composed of different phases along with a β-CoAl depleted zone in oxidized bond coat. Aluminum diffuses from β-CoAl for the formation and growth of alumina scale, thereby, causing a depletion of the β phase in the near surface of the bond coat. The composition of different phases in the oxide scale (labeled as 1, 2 and 3) are summarized in Table 3. The dark phase labeled as (1) was found to be Al and O reach and the other two phases labeled as (2) and (3) were found to be mixed oxides which formed on top of Al_2O_3 scale whose compositions were shown in Table 3.

A detailed microstructure and compositional analysis of the oxidized top surface of CoNiCrAlY bond coat was undertaken to observe the morphology and composition of oxide scale. Fig. 8a to e show the scanning electron micrographs of the top surface of bare bond coat after isothermal oxidation at 1000 °C for 96 hours, showing (a) oxidized top surface at low magnification and high magnification view of (b) region 1, (c) region 2, (d) region 3 and (e) region 4, respectively. The EDS analysis of the different regions as labeled in Fig. 8a is summarized in Table 4. From Table 4 it may be noted that the zone labeled as 1 (shown in Fig. 8b) contains oxides of chromium. From Fig. 8b it may further be concluded that the morphology of chromium oxides are granular and contains a significant volume fraction of porosities, The size of the oxide particles ranges from 100 nm to 3 μm. The zone labeled as 2 (cf. Fig. 8c) is porous spinel oxides which is having a polygonal morphology, with the chemical formula near equivalent to $CoCr_2O_4$ (as confirmed by x-ray diffraction study) and supported by the composition analysis as summarized in Table 4. The zone labeled as 3 (cf. Fig. 8d) is enriched in αAl_2O_3 with trigonal crystal structure. The morphology of the oxide particles is elongated with a high aspect ratio and with uniform particle size/ aspect ratio. From the detailed EDS analysis (as summarized in Table 4) and XRD result, it is confirmed that the oxide is Al_2O_3. The region 4 (as

shown in Fig. 8e) contains polyhedral shaped oxides whose composition analysis shows mixed oxides of Co and Ni, whose presence is also confirmed by XRD analysis (cf. Fig. 9 and Fig. 10).

3.3.2. X-ray diffraction analysis

Fig. 9 shows the x-ray diffraction profiles of the top surface of as-sprayed (plot 1) and as-oxidized CoNiCrAlY bond coat at 900 °C for 24 hours (plot 2), 900 °C for 96 hours (plot 3) and at 1000 °C for 96 hours (plot 4). From plot 1, it may be noted that the as-sprayed bond coat consists of γ/γ' matrix and β-CoAl phases. The β phase acts as an aluminum reservoir and helps in protecting the surface from oxidation [35]. From plot 2, it may be observed that after oxidation, there is formation of Al_2O_3, CoO, $CoCr_2O_4$, $NiCr_2O_4$, $NiAl_2O_4$, and $CoAl_2O_4$ phases. A close comparison between plot 1 and plot 2 revealed that β phase was absent in as-oxidized surface, which is possibly attributed to the consumption of Al present in the β phase for the formation of Al_2O_3. From plot 3, it is evident that along with Al_2O_3, there is presence of other spinel oxides such as $NiAl_2O_4$ and $CoAl_2O_4$, which make the oxide scale less protective as they are porous and non adherent in nature [46]. Due to increase in oxidation temperature to 1000 °C (plot 4), apart from formation of Al_2O_3, CoO, $CoCr_2O_4$, $NiCr_2O_4$, $NiAl_2O_4$, and $CoAl_2O_4$ phases, Cr_2O_3 phase was also formed as shown in plot 4. The intensities of the oxides were also found to increase with increase in the oxidation temperature due to increased quantity of oxide formation at increased temperature of oxidation.

Fig. 10 shows the mass fraction of different phases present in the as-received CoNiCrAlY bond coat and the same after isothermal oxidation at 900 °C for 24 hours, 900 °C for 96 hours and 1000 °C for 96 hours. From Fig. 10, it can be seen that the as-received CoNiCrAlY bond

coat contains γ–Co matrix and β–CoAl phase which is also confirmed by XRD analysis. After oxidation at 900 °C for 24 hour and 96 hour, the Co and Al present in the bond coat alloy get oxidized to form their respective oxides. From the mass fraction calculation of different phases after thermal exposure at 900 °C for 24 hour and 96 hour, it may be observed that mass fraction of γ –Co initially decreased and then increased up to 96 hour oxidation. The initial decrease in volume fraction of γ-Co phase may be attributed to the oxidation of Co which resulted in the formation of CoO. Increase in the mass fraction of γ – Co at the later stage may be attributed to formation of the oxide scale with non-uniform thickness. The mass fractions of CoO and Al_2O_3 were found to decrease with time of exposure, which might be attributed to the formation of spinel oxide. As the temperature of oxidation is increased to 1000 °C, the kinetics of oxide formation is increased. Co and Al present in the bond coat alloy get oxidized to form its corresponding oxides. Comparing mass fractions of different phases after thermal exposure at 900 °C for 96 hours and 1000 °C for 96 hours, it may be noted that mass fraction of γ – Co decreases with increase in temperature. The decreased mass fraction of γ – Co with increase in temperature is attributed to oxidation of Co to form CoO. The mass fractions of CoO and Al_2O_3 were found to increase with increase in temperature, which may be due to increased kinetics of growth of CoO and Al_2O_3 with increase in temperature.

Fig. 11 shows the x-ray diffraction profiles of duplex TBC in as-sprayed condition (plot 1) and the same after isothermal oxidation at 900 °C for 24 hrs (plot 2) and 900 °C for 96 hrs (plot 3) and 1000 °C for 96 hours (plot 4). From Fig. 11 it may be noted that due to oxidation, there is no change in phase distribution in the coated surface. Hence, it may be concluded that the thermal barrier coating developed in the present study remains stable up to 96 hrs of thermal exposure at both 900 °C and 1000 °C.

Fig. 12 shows the x-ray diffraction profiles of the compositionally graded thermal barrier coating after isothermal oxidation at 900 °C for 96 hours with 100% YSZ (plot 1), 70% YSZ + 30% CoNiCrAlY (plot 2), 50% YSZ + 50% CoNiCrAlY (plot 3), and 30% YSZ + 70% CoNiCrAlY (plot 4). In the microstructure of the top layer, i.e. 100% YSZ, there is presence of only t'-ZrO_2 as was observed for duplex TBC. However, with depth there are formation of oxide of aluminium (Al_2O_3), cobalt (CoO) and spinels of nickel – chromium oxide ($NiCr_2O_4$), colablt – chromium oxide ($CoCr_2O_4$), nickel – aluminium oxide ($NiAl_2O_4$) and cobalt – aluminium oxide ($CoAl_2O_4$) along with the presence of t'-ZrO_2 phase. The peak intensities of t'-ZrO_2 phase decrease and metallic oxides/spinels (Al_2O_3, CoO, $NiAl_2O_4$ and $CoAl_2O_4$) increase with depth of the coating. However, there was no signature of the presence of $NiCr_2O_4$ and $CoCr_2O_4$ peaks in plot 3 and 4, which concludes that with increase in depth the tendency to spinel formation and its kinetics decrease.

Fig.13 shows the mass fraction of different phases present in graded TBC layers after isothermal oxidation at 900 °C for 96 hours. From Fig. 13, it may be noted that the mass fraction of t'-ZrO_2 and γ-Co phase decrease with depth and the mass fraction of CoO and Al_2O_3 phase increase with depth. The mass fractions of CoO and Al_2O_3 phase increases with increase with increase in depth which is due to the availability of more metallic CoNiCrAlY alloy with depth. Fig. 14 shows the x-ray diffraction profiles of each graded layers after isothermal oxidation at 1000 °C for 96 hour. From plot 1, it can be seen that the top 100% YSZ contains the same phase as it was in case of as-sprayed coating. The composite layers contain different types of oxides such as Al_2O_3, $CoAl_2O_4$, $NiAl_2O_4$, $CoCr_2O_4$, and $NiCr_2O_4$ as shown in Fig. 14. Fig. 15 compares the mass fraction of different phases formed in bond coat and graded thermal barrier coating for isothermal exposure in 1000 °C for 96 hours. From Fig. 15, it may be noted that the mass

fraction of CoO phase increases with depth. This may be due to the presence of higher metallic CoNiCrAlY percentage in the graded layer which increases with depth. The mass fraction of Al_2O_3 phase initially increases with depth and then finally decreases up to 30% YSZ + 70% CoNiCrAlY layer as observed from Fig. 15.

3.3.3 Mechanism of Oxidation

The formation of different oxides at the bond coat-top coat interface as well as in the graded layers may be explained from the standard free energy of individual oxide formation as shown in Table 5 [47].

The minimum thermodynamic activity of the elements to form their corresponding oxides may be calculated from the following equations and are summarized in Table 5 [47].

$$\Delta G^0 = -RT \ln K_1 = -RT \ln \left[\frac{\left(a_{Al_2O_3} \right)}{\left(a_{Al} \right)^2 \left(P_{O_2} \right)^{3/2}} \right] \quad (2)$$

$$\Delta G^0 = -RT \ln K_2 = -RT \ln \left[\frac{\left(a_{Cr_2O_3} \right)}{\left(a_{Cr} \right)^2 \left(P_{O_2} \right)^{3/2}} \right] \quad (3)$$

$$\Delta G^0 = -RT \ln K_3 = -RT \ln \left[\frac{\left(a_{CoO} \right)}{\left(a_{Co} \right) \left(P_{O_2} \right)^{1/2}} \right] \quad (4)$$

$$\Delta G^0 = -RT \ln K_4 = -RT \ln \left[\frac{\left(a_{NiO} \right)}{\left(a_{Ni} \right) \left(P_{O_2} \right)^{1/2}} \right] \quad (5)$$

where, a represents the thermodynamic activity of concerned phase shown as the subscript and K_1, K_2, K_3, and K_4 represents the equilibrium constant for the reactions (2) – (5). Table 5 summarizes the standard Gibb's free energy of formation of different oxides and minimum thermodynamic activity of elements required to form their respective oxides at P_{O2} = 1 atm. From Table 5, it may be concluded that among all oxides, Al_2O_3 is the preferred oxide to be formed initially. Furthermore, from Table 5 it is also evident that the minimum thermodynamic activity required for the formation of their respective oxide is lowest in aluminium. Hence, Al_2O_3 is the preferred oxide to form at the bond coat-top coat interface as well as in the graded layers. In the onset of oxidation, growth of TGO was faster due to rapid oxidation of aluminium present in CoNiCrAlY. At later stage of oxidation, a protective Al_2O_3 scale was formed and thereby, reducing TGO growth rate. As soon as the aluminium concentration in the CoNiCrAlY bond coat decreases below its critical value to form protective alumina scale, other elements such as Cr, Co, and Ni migrate towards oxide-gas interface to form Cr_2O_3, CoO, and NiO scales according to their standard free energy of formation and minimum thermodynamic activities of elements required for the formation of their oxides as summarized in Table 5. The formation of these oxides was followed by formation of various spinel oxides such as $CoAl_2O_4$, $NiAl_2O_4$, $CoCr_2O_4$, and $NiCr_2O_4$ according to their standard free energy of formation as summarized in Table 5. The measured thickness of TGO at different time intervals includes thickness of both Al_2O_3 and other spinel oxides. The formation of these oxides in the graded layers helps to reduce oxygen diffusion and in turn lowering the growth rate of TGO in compositionally graded TBC. The formation of these spinel oxides requires high oxygen activity and as a result of which these oxides formed on top of already grown Al_2O_3 scales. In compositionally graded TBC, the oxygen activity at bond coat-top coat interface is less as compared to duplex TBC as the graded layer

which was oxidized during exposure at elevated temperature reduces the oxygen ingress towards bond coat-top coat interface. This helps to reduce the quantity of detrimental spinel oxide formation as these oxides grow under high oxygen activity [48]. This attributes to the lower growth rate of TGO in graded TBC than duplex TBC.

Fig. 16 compares the schematic representation of different stages of oxidation in (a) CoNiCrAlY coated Inconel substrate, and the same after (b) duplex TBC coating and (c) graded TBC coating, where, T_0 represents the schematic of as-coated sample and (T_1 to T_4) represents the different stages of oxidation with increase in temperature or time of isothermal exposure in air. In the onset of oxidation, at T_1, thin Al_2O_3 scale forms due to oxidation of Al at the surface of bare bond coat or at the interface between the top coat and bond coat of duplex and at the interface or between top coat and bond coat along with along different layers of graded TBC. As soon as a thin Al_2O_3 scale forms on the surface of CoNiCrAlY, the Cr, Co and Ni ions diffuse through the Al_2O_3 scale to form CoO, NiO and Cr_2O_3 along with Al_2O_3 at T_2 according to Table 5. At T_3, $CoAl_2O_4$, $NiAl_2O_4$, $CoCr_2O_4$, and $NiCr_2O_4$ spinel oxides form along with Al_2O_3 according to Table 5.

3.3.4. Residual stress analysis

Residual stress plays an important role in determining the service life of the coating. Residual stress may be developed in plasma sprayed thermal barrier coating due to a large quenching rate arising out from deposition of coating and its solidification. On the other hand, when the coated surface is subjected to isothermal heating, there is formation of TGO which also introduces residual stress in the coated surface. The quenching stress (σ_q) arises because of large temperature difference experienced during deposition of coating (Eq 6) and the thermal stress

(σ_t) arises as a result of thermal expansion mismatch between the substrate and coating during cooling (Eq 7).

$$\sigma_q = \alpha_c E_c \left(T_m - T_s\right) \quad (6)$$

and

$$\sigma_t = \frac{E_c \left(\alpha_c - \alpha_s\right)\left(T_d - T_a\right)}{1 - \nu_c} \quad (7)$$

where, α_c and α_s are the coefficient of thermal expansion of coating and substrate, respectively. T_m, T_s, T_d and T_a are the melting temperature of coating material, substrate temperature, deposition temperature and ambient temperature, respectively. E_c and υ_c are the Young's modulus and Poisson's ratio of the coating. The residual stress introduced in the coating (both the duplex and graded) in as-received state and the same after isothermal oxidation at 900 °C and 1000 °C are summarized in Table 6 and Table 7, respectively. From Table 6 and 7, it can be seen that the residual stress developed on the surface of the as-deposited thermal barrier coating (100 % YSZ) is tensile. The tensile nature of residual stress is attributed to rapid quenching of molten splats from melting temperature to the substrate temperature. After isothermal exposure at 900 °C, the residual stress in 100% YSZ coating initially decreases up to 24 hours of exposure and then increases with increase in time. The initial decrease in residual stress with isothermal exposure for short duration is attributed to release in quench stress, which increases further with increase in time, possibly due to growth of TGO film. With increase in depth, there is introduction of compressive residual stress, the magnitude of which increases with increase in depth. The increased magnitude of residual compressive stress with increase in the metallic percentage in the composite layer is due to a large difference in coefficient of thermal expansion

between the ceramic (YSZ) and metallic CoNiCrAlY. Furthermore, the compressive stress developed in the below surface layer increases with increase in time of exposure. Fig. 17 shows the schematic representation of variation of coefficient of thermal expansion (α) and Young's modulus (E) of (a) duplex and (b) compositionally graded TBC. The coefficient of thermal expansion, α, increases with increase in the metallic CoNiCrAlY content in the coating due to a higher α of CoNiCrAlY than ceramic materials. Similarly, the Young's modulus (E) increases with increase in the metallic CoNiCrAlY content in the composite layer as the addition of metallic CoNiCrAlY decreases the defect (porosity, microcracks etc.) content in the composite layer [9]. From Eq 15, it is also evident that the residual stress in the graded layers increases with increase in the metallic content. The effect of porosity on residual stress has been studied by Portinha et al. [49] which showed an increase in compressive stress due to decrease in porosity content in the coating. With increase in thermal exposure, the metallic CoNiCrAlY gets oxidized and the formation of oxides produce strain in the composite layer which leads to increase in the value of Young's modulus of the composite layer, and thereby, increasing the residual compressive stress as shown in Table 6 and 7.

It is relevant to mention that at low temperature of exposure, the underlying splats or substrate contributes to the development of tensile stress in the coating. The magnitude of the residual stress on the surface of 100% YSZ thermal barrier coating shows tensile nature with increase in the time of thermal exposure. On the other hand, the graded composite layers show compressive residual stress. The 70% YSZ + 30% CoNiCrAlY graded layer shows compressive stress developed on it which increases with time and temperature. A close comparison between the residual stress of the 100% YSZ layer and 70% YSZ + 30% CoNiCrAlY layer shows that the tensile residual stress in the 100% YSZ layer which increases with time and temperature is due to

the underlying 70% YSZ + 30% CoNiCrAlY layer whose compressive stress increases with time and temperature. The compressive nature of residual stress in composite layers is attributed to the thermal stress developed due to the thermal expansion mismatch between CoNiCrAlY and YSZ. By looking into the residual stress component $\sigma_{11,}$ it can be seen that the residual stress in the graded layer changes from tensile in 100% YSZ to compressive in following graded layers till bond coat.

4. Conclusions

In the present study, the isothermal oxidation behavior of the duplex as well as compositionally graded thermal barrier coating has been conducted at three reference temperatures 900 °C, 950 °C and 1000 °C from 24 hours to 96 hours. From the detailed investigations, the following conclusions may be drawn:

1. The microstructure of plasma sprayed 100% YSZ coating consists of porosities and micro-cracks which help the coating to be strain tolerant, however, allow oxygen to diffuse through it leading to oxidation of bond coat.
2. The as-received microstructure of CoNiCrAlY bond coat shows a dual phase microstructure of γ/γ' matrix and β - CoAl.
3. The kinetics of growth of the TGO is parabolic in nature both in duplex and compositionally graded TBC at 900 °C, 950 °C and 1000 °C. The growth rate TGO in compositionally graded TBC have been found to be slower than duplex TBC at 900 °C, 950 °C and 1000 °C. The activation energy of duplex and compositionally graded TBC was found to be 129 kJ/mol and 175 kJ/mol, respectively.

4. Post-oxidation analysis of TGO shows the formation of Al_2O_3 and spinel oxides of Co, Ni, Cr, and Al. The top surface of oxidized bare bond coat contains Al_2O_3, Cr_2O_3, $CoCr_2O_4$, $NiCr_2O_4$, $CoAl_2O_4$, and $NiAl_2O_4$.
5. The residual stress in 100% YSZ of as-received graded TBC shows tensile nature. The isothermal exposure of as-received graded TBC at 900 °C for 24 hour and 72 hour shows tensile nature of residual stress with no significant variation of its magnitude with time of exposure. The magnitude of tensile stress in 100% YSZ, however, increased with increase in temperature of exposure. On the other hand, the graded composite layers showed compressive residual stress. The graded layer shows compressive stress which increases with time and temperature.

Acknowledgements

The partial financial support from the Department of Science and Technology (DST), New Delhi, Council of Scientific and Industrial Research, N. Delhi and Indian Space Research Organization (ISRO) are gratefully acknowledged.

References

1. W. R Chen, X. Wu, B. R. Marple, P. C. Patnaik, Oxidation and crack nucleation/growth in an air-plasma-sprayed thermal barrier coating with NiCrAlY bond coat Surf. Coat. Technol. 197 (2005) 109-115.
2. A. Rico, J. Gómez-García, C.J. Múnez, P. Poza, V. Utrilla, Mechanical properties of thermal barrier coatings after isothermal oxidation: Depth sensing indentation analysis Surf. Coat. Technol. 203 (2009) 2307-2314.
3. A. Bolcavage, A. Feuerstein, J. Foster, P. Moore, Thermal shock testing of thermal barrier coating/bondcoat systems, J. Mater. Eng. Perform. 30 (2004) 389-397.

4. W.Y. Lee, D.P. Stinton, C.C. Berndt, F. Erdogan, Y.D. Lee, Z. Mutasim, Concept of functionally graded materials for advanced thermal barrier coating applications: A review, J. Am. Ceram. Soc. 79 (1996) 3003-3012.

5. A.S. Demirkiran, E. Avci, Evaluation of Functionally Gradient Coatings Produced by Plasma-Spray Technique, Surf. Coat. Technol. 116 (1999) 292-295.

6. A Kawasaki, R Watanabe, Thermal fracture behavior of metal/ceramic functionally graded materials, Eng. Fract. Mech. 69 (2002) 1713-1728.

7. K.A. Khor, Y.W. Zu, Effects of residual stress on the performance of plasma sprayed functionally graded ZrO_2: NiCoCrAlY coatings, Mater. Sci. Eng., A 277 (2000) 64-76.

8. K.A. Khor, Z.L. Dong, Y.W. Zu, Plasma sprayed functionally graded thermal barrier coatings, Mater. Lett. 38 (1999) 437-444.

9. K.A. Khor, Y.W. Zu, Thermal properties of plasma-sprayed functionally graded thermal barrier coatings, Thin Solid Films 372 (2000) 104-113.

10. K.A. Khor, Z.L. Dong, Y.W. Zu, Influence of oxide mixtures on mechanical properties of plasma sprayed functionally graded coating, Thin Solid Films 368 (2000) 86-92.

11. Z.L. Dong, K.A. Khor, Y.W. Zu, Microstructure formation in plasma-sprayed functionally graded NiCoCrAlY/yttria-stabilized zirconia coatings, Surf. Coat. Technol. 114 (1999) 181-186.

12. K.A. Khor, Y.W. Zu, Z.L. Dong, Plasma spraying of functionally graded yttria stabilized zirconia/NiCoCrAlY coating system using composite powders, J. Therm. Spray Technol. 9 (2000) 245-249.

13. J. Yao, Y. He, D. Wang, H. Peng, H. Guo, S.Gong, Thermal barrier coating bonded by (Al_2O_3–Y_2O_3)/(Y_2O_3-stabilized ZrO_2) laminated composite coating prepared by two-step cyclic spray pyrolysis, Corros. Sci. 80 (2014) 37–45.

14. K. Shirvani, S. Mastali, A. Rashidghamat, H. Abdollahpour, The effect of silicon on thermal shock performance of aluminide-thermal barrier coatings, Corros. Sci. 75 (2013) 142–147.

15. J. He, Y. Luan, H. Guo, H. Peng, Y. Zhang, T. Zhang, S. Gong, The role of Cr and Si in affecting high-temperature oxidation behavior of minor Dy doped NiAl alloys, Corros. Sci. 77 (2013) 322–333.

16. C.Z. Xu, S.M. Jiang, Z.B. Bao, J. Gong, C. Sun, Isothermal oxidation behaviour of a gradient NiCoCrAlSiY coating deposited by arc ion plating on a Ni-based single crystal superalloy, Corros. Sci. 51 (2009) 1467–1474.

17. Y.N. Wu, P.L. Ke, Q.M. Wang, C. Sun, F.H. Wang, High temperature properties of thermal barrier coatings obtained by detonation spraying, Corros. Sci. 46 (2004) 2925–2935.

18. W.Z. Li, Y.Q. Li, Q.M. Wang, C. Sun, X. Jiang, Oxidation of a NiCrAlYSi overlayer with or without a diffusion barrier deposited by one-step arc ion plating, Corros. Sci. 52 (2010) 1753–1761.

19. H.Q. Li, Q.M. Wang, S.M. Jiang, J. Ma, J. Gong, C. Sun, Oxidation and interfacial fracture behaviour of NiCrAlY/Al_2O_3 coatings on an orthorhombic-Ti_2AlNb alloy, Corros. Sci. 53 (2011) 1097–1106.

20. F.H. Yuan, Z.X. Chen, Z.W. Huang, Z.G. Wang, S.J. Zhu, Oxidation behavior of thermal barrier coatings with HVOF and detonation-sprayed NiCrAlY bondcoats, Corros. Sci. 50 (2008) 1608–1617.

21. M.A. Helminiak, N.M. Yanar, F.S. Pettit, T.A. Taylor, G.H. Meier, The behavior of high-purity, low-density air plasma sprayed thermal barrier coatings, Surf. Coat. Technol. 204 (2009) 793–796.

22. J. Yao, Y. He, D. Wang, J. Lin, High-temperature oxidation resistance of (Al_2O_3–Y_2O_3)/(Y_2O_3-stabilized ZrO_2) laminated coating on 8Nb–TiAl alloy prepared by a novel spray Pyrolysis, Corros. Sci. 80 (2014) 19–27.

23. P. Chagnon and P. Fauchais, Thermal spraying of ceramics, Ceram. Int. 10 (1984) 119-131.

24. L. Pawlowski, The Science and Engineering of Thermal Spray Coating, second ed., John Wiley and Sons Ltd, England, 2008.

25. A.G. Evans, D.R. Clarke, C.G. Levi, The influence of oxides on the performance of advanced gas turbines, J. Eur. Ceram. Soc. 28 (2008) 1405-1419.

26. A. Kulkarni, J. Gutleber, S. Sampath, A. Goland, W.B. Lindquist, H. Herman, A.J. Allen, B. Dowd, Studies of the microstructure and properties of dense ceramic coatings produced by high-velocity oxygen-fuel combustion spraying, Mater. Sci. Eng., A 369 (2004) 124-137.

27. D.E. Crawmer, Thermal spray processes, in: J.R. Davis (Ed.), Handbook of Thermal Spray Technology, Thermal Spray Society and ASM International, Metals Park, OH, 2004, pp. 54-76.

28. P. Sharma, J. Dutta Majumdar, Surface characterization and mechanical properties evaluation of boride-dispersed nickel-based coatings deposited on copper through thermal spray routes, J. Therm. Spray Technol. 21 (2012) 800-809.

29. P. Sharma, J. Dutta Majumdar, Microstructural characterization and properties evaluation of ni-based hardfaced coating on AISI 304 stainless steel by high velocity oxy-fuel coating technique, Metall. Mater. Trans. A 44 (2013) 372-380.

30. S. Nath, I. Manna, J. Dutta Majumdar, Compositionally graded thermal barrier coating by hybrid thermal spraying route and its non-isothermal oxidation behavior, J. Therm. Spray Technol. 22 (2013) 901-917.

31. B.D. Cullity, Elements of X-ray Diffraction, second ed., Addison-Wesley, Menlo Park, CA, 1956.

32. Z. Wang, A. Kulkarni, S. Deshpande, T. Nakamura, H. Herman, Effects of pores and interfaces on effective properties of plasma sprayed zirconia coatings, Acta Mater. 51 (2003) 5319–5334. L

33. A. Kulkarni, A. Vaidya, A. Goland, S. Sampath, H. Herman, Processing effects on porosity-property correlations in plasma sprayed yttria-stabilized zirconia coatings, Mater. Sci. Eng. A 359 (2003) 100-111.

34. A. D. Jadhav, N. P. Padture, E. H. Jordan, M. Gell, P. Miranzo, E. R. Fuller Jr., Low-thermal-conductivity plasma-sprayed thermal barrier coatings with engineered microstructures, Acta Mater. 54 (2006) 3343–3349.

35. P. Richer, M. Yandouzi, L. Beauvais, B. Jodoin, Oxidation behaviour of CoNiCrAlY bond coats produced by plasma, HVOF and cold gas dynamic spraying**,** Surface & Coatings Technology 204 (2010) 3962–3974.

36. M. Madhwal, E. H. Jordan, M. Gell, Failure mechanisms of dense vertically-cracked thermal barrier coatings, Mater. Sci. Eng. A 384 (2004) 151–161.

37. W.R. Chena, X. Wua, B.R. Marpleb, P.C. Patnaik, Oxidation and crack nucleation/growth in an air-plasma-sprayed thermal barrier coating with NiCrAlY bond coat, Surf. Coat. Technol. 197 (2005) 109– 115.

38. A.C. Fox, T.W. Clyne, Oxygen transport by gas permeation through the zirconia layer in plasma sprayed thermal barrier coatings, Surf. Coat. Technol. 184 (2004) 311-321.

39. B.C. Wu, E. Chang, D. Tu, S.L. Wang, Microstructures, properties and failure analysis of (ZrO_2-8wt.%Y_2O_3) / ((Co, Ni)-Cr-AI-Y) Thermal barrier coatings, Mater. Sci. Eng. A 111 (1989) 201-210.

40. Y. J. Su, R. W. Trice, K. T. Faber, $ H. Wang, W. D. Porter, Thermal conductivity, phase stability, and oxidation resistance of $Y_3Al_5O_{12}$ (YAG)/Y_2O_3–ZrO_2 (YSZ) thermal barrier coatings, Oxd. Met. 61 (2004) 253-271.

41. S. Sridharan, L. Xie, E. H. Jordan, M. Gell, K.S. Murphy, Damage evolution in an electron beam physical vapor deposited thermal barrier coating as a function of cycle temperature and time, Mater. Sci. Eng. A 393 (2005) 51-62.

42. W.R. Chen, X. Wu, B.R. Marple, P.C. Patnaik, Oxidation and crack nucleation/growth in an air-plasma-sprayed thermal barrier coating with NiCrAlY bond coat, Surf. Coat. Technol. 197 (2005) 109-115.

43. F.H. Yuan, Z.X. Chen, Z.W. Huang, Z.G. Wang, S.J. Zhu, Oxidation behavior of thermal barrier coatings with HVOF and detonation-sprayed NiCrAlY bondcoats, Corros. Sci. 50 (2008) 1608-1617.

44. D. Seo, K. Ogawa, Y. Nakao, H. Miura, T. Shoji, Influence of high-temperature creep stress on growth of thermally grown oxide in thermal barrier coatings, Surf. Coat. Technol. 203 (2009) 1979-1983.

45. P.K. Wright, A.G. Evans, Mechanisms governing the performance of thermal barrier coatings, Curr. Opin. Solid State Mater. Sci. 4 (1999) 255-265.

46. Y. Li, C. Li, Q. Zhang, L. Xing, G. Yang, Effect of chemical compositions and surface morphologies of MCrAlY coating on its isothermal oxidation behavior, J. Therm. Spray Technol. 20 (2011) 121-131.

47. W.F. Gale, T.C. Totemeir, Smithell metal reference book, eighth edition, Elsevier, Burlington, USA, 2008.

48. F. Tang, L. Ajdelsztajn, J. M. Schoenung, Characterization of oxide scales formed on HVOF NiCrAlY coating with various oxygen contents introduced during thermal spraying, Scripta Mater. 51 (2004) 25-29.

49. A. Portinha, V. Teixeira, J. Carneiro, M.G. Beghi, C.E. Bottani, N. Franco, R. Vassen, D. Strover, A.D. Sequeira, Residual stresses and elastic modulus of thermal barrier coatings graded in porosity, Surf. Coat. Technol. 188-189 (2004) 120-128.

List of Figures

Fig. 12. X-ray diffraction profiles of the graded thermal barrier coating layers after isothermal oxidation at 900 °C for 96 hours with 100% YSZ (plot 1), 70% YSZ + 30% CoNiCrAlY (plot 2), 50% YSZ + 50% CoNiCrAlY (plot 3), and 30% YSZ + 70% CoNiCrAlY (plot 4).

Fig.13. Mass fraction of different phases present in graded TBC layers after isothermal oxidation at 900 °C for 96 hours.

Fig. 14. X-ray diffraction profiles of the graded thermal barrier coating layers after isothermal oxidation at 1000 °C for 96 hours with 100% YSZ (plot 1), 70% YSZ + 30% CoNiCrAlY (plot 2), 50% YSZ + 50% CoNiCrAlY (plot 3), and 30% YSZ + 70% CoNiCrAlY (plot 4).

Fig. 15. Mass fraction of different phases present in graded TBC layers after isothermal oxidation at 1000 °C for 96 hours.

Fig. 16. Schematic representation of mechanism of oxidation in (a) bare bond coat, (b) duplex TBC, and (c) compositionally graded TBC.

Fig. 17. Schematic representation of thermal expansion and Young's modulus in (a) duplex thermal barrier coating and (b) compositionally graded thermal barrier coating.

List of Tables

Table 1: EDS compositional analysis (atomic %) of different zones observed in Fig. 2.

Table 2: Rate constant and activation energy values for duplex and compositionally graded thermal barrier coating system.

Table 3: EDS compositional analysis (atomic %) of oxides scales formed on the cross-section of bare bond coat oxidized at 1000 °C for 96 hours as shown in Fig. 7b.

Table 4: EDS compositional analysis (atomic %) of different oxides formed on top of bare bond coat oxidized at 1000 °C for 96 hours as shown in Fig. 8a.

Table 5: Gibb's free energy of formation and thermodynamic activity of elements present in the bond coat alloy to form their respective oxides at $P_{O2} = 1$ atm.

Table 6: Residual stress after isothermal oxidation at 900 °C in compositionally graded TBC.

Table 7: Residual stress after isothermal oxidation at 1000 °C in compositionally graded TBC.

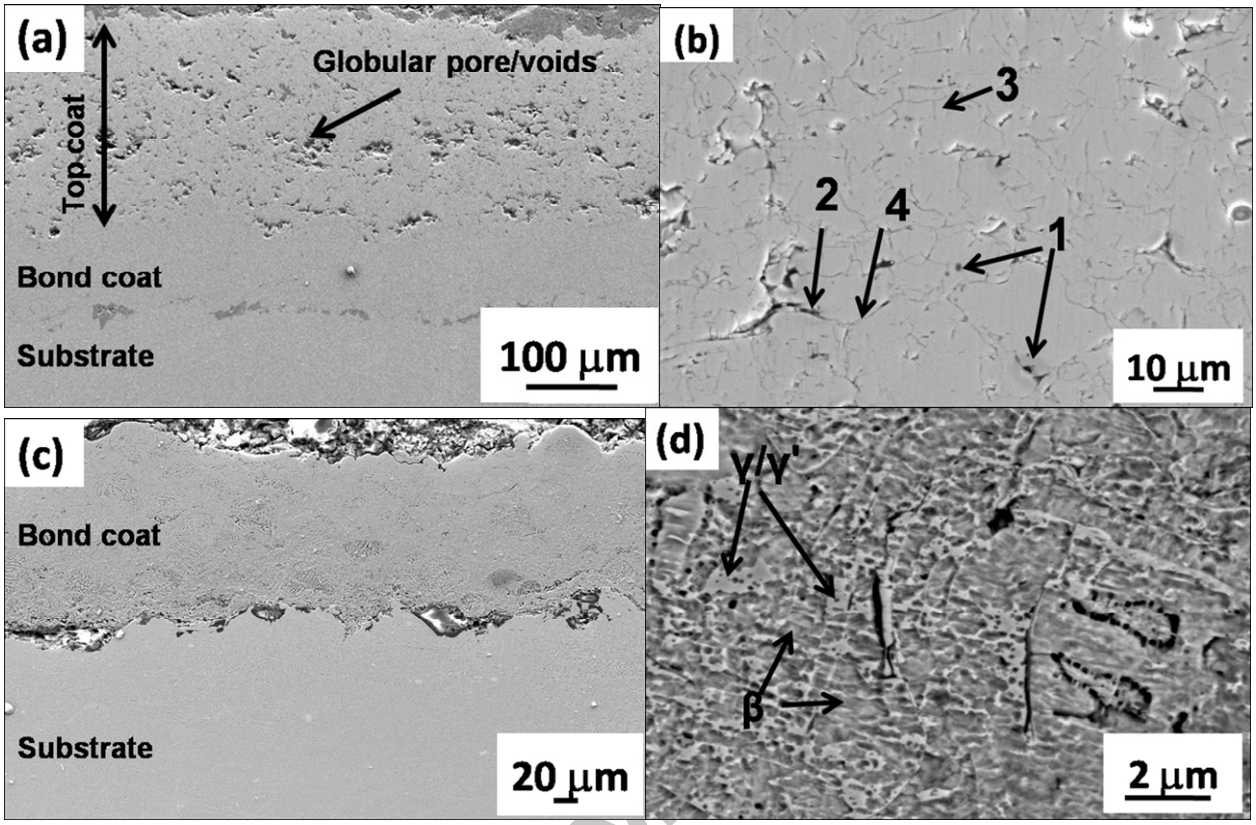

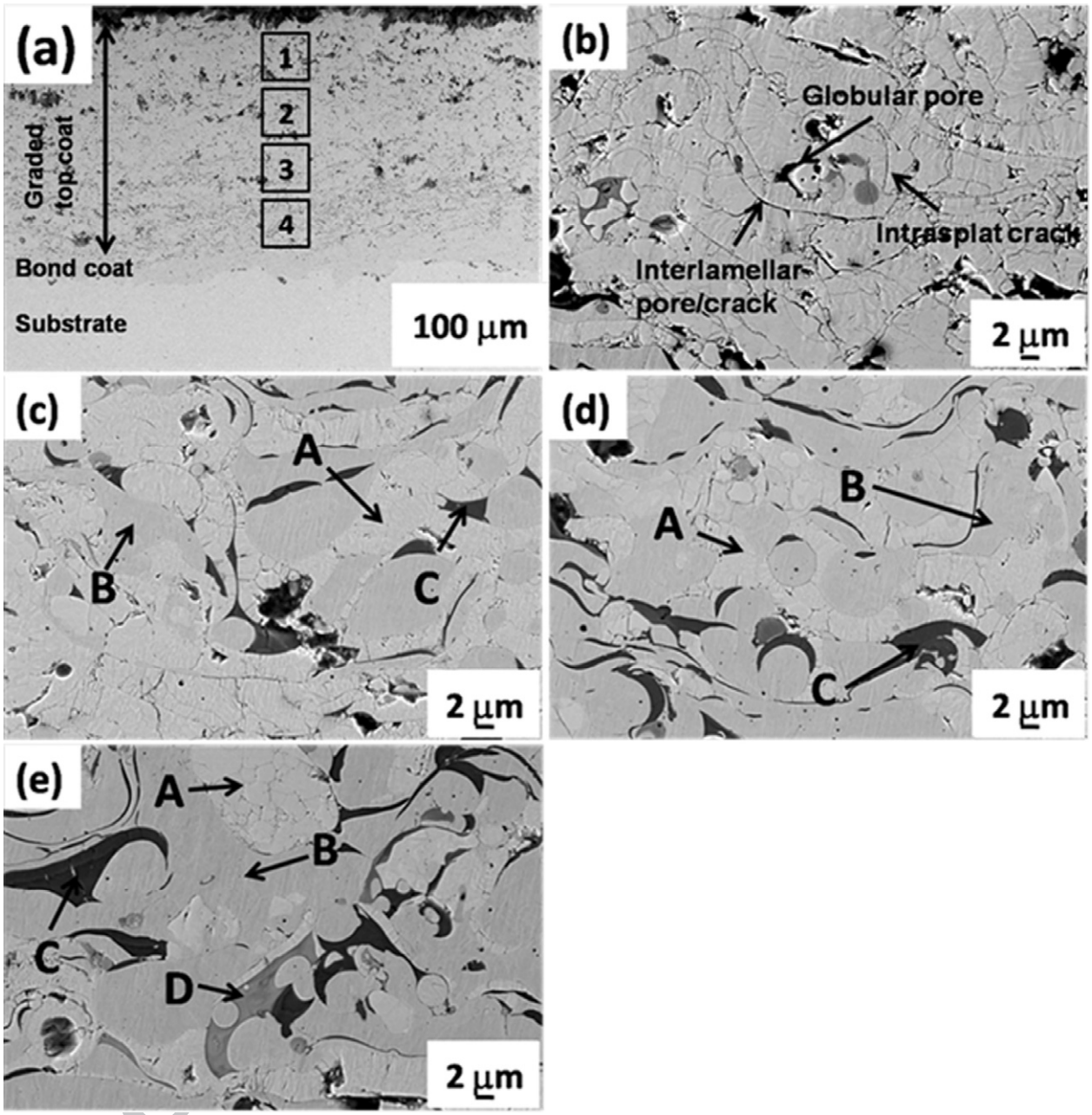
(a)
1
2
3
4
Graded top coat
Bond coat
Substrate
100 μm
(b)
Globular pore
Intrasplat crack
Interlamellar pore/crack
2 μm
(c)
A
B
C
2 μm
(d)
A
B
C
2 μm
(e)
A
B
C
D
2 μm

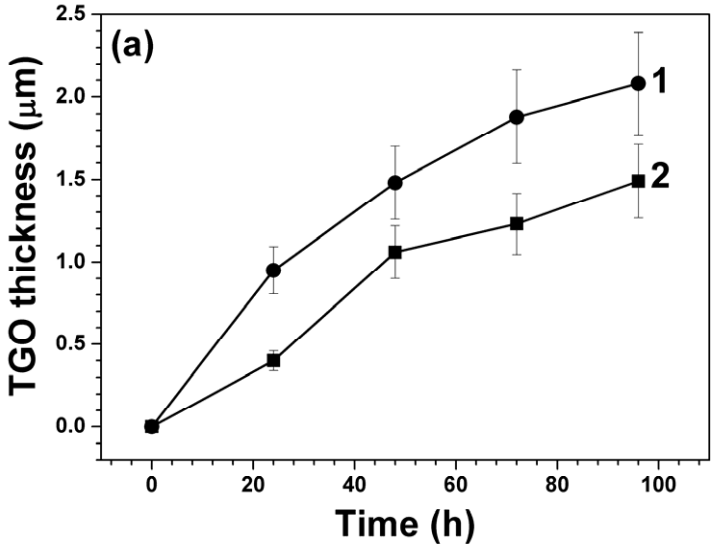
(a)
TGO thickness (μm)
Time (h)
1
2

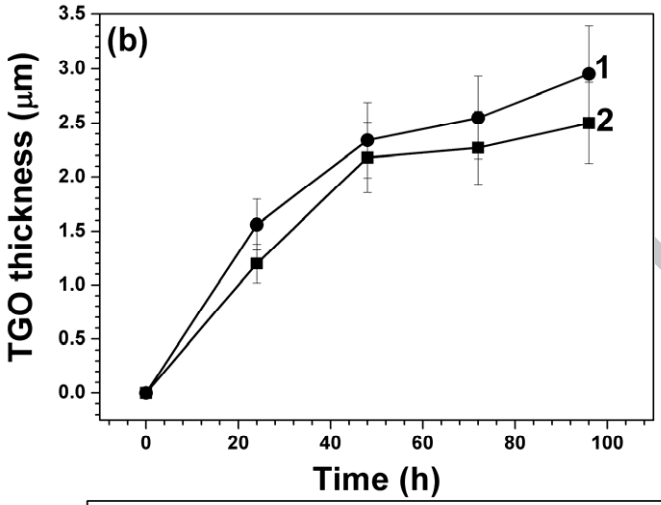
(b)
TGO thickness (μm)
Time (h)
1
2

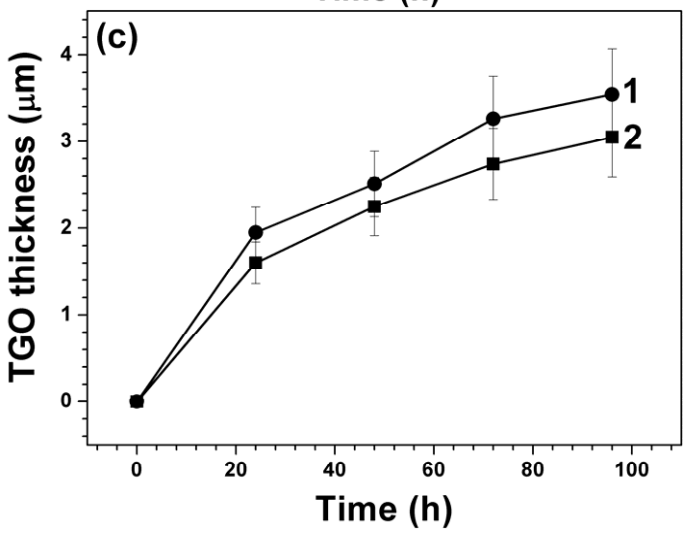
(c)
TGO thickness (μm)
Time (h)
1
2

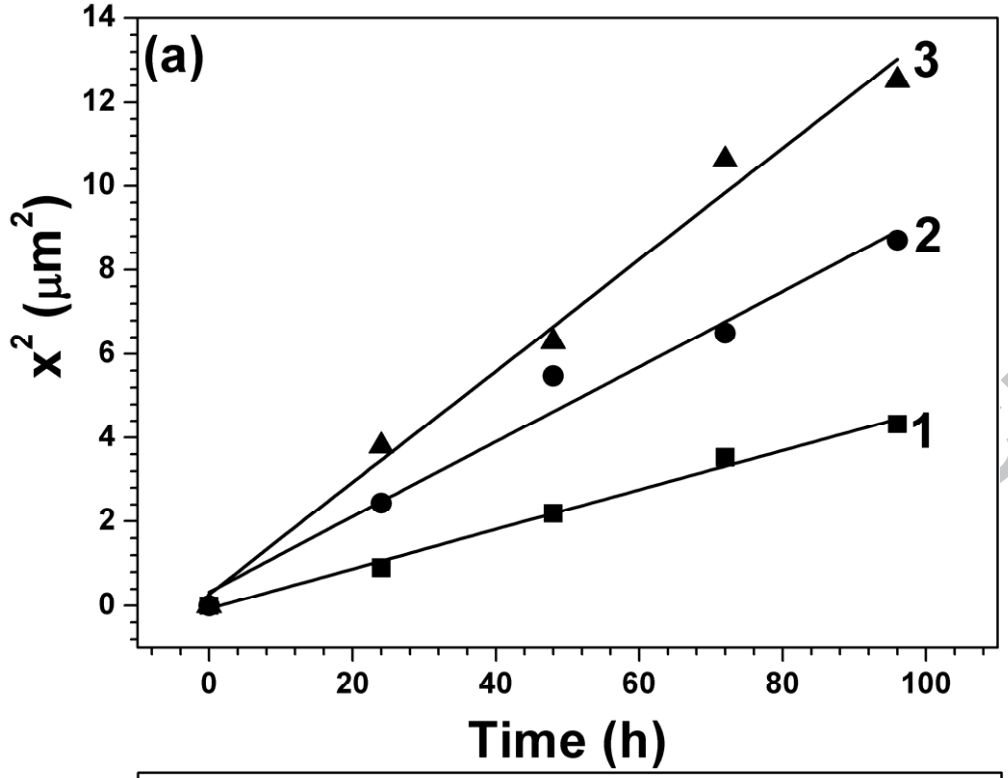
(a)
x^2 (μm^2)
Time (h)
1
2
3

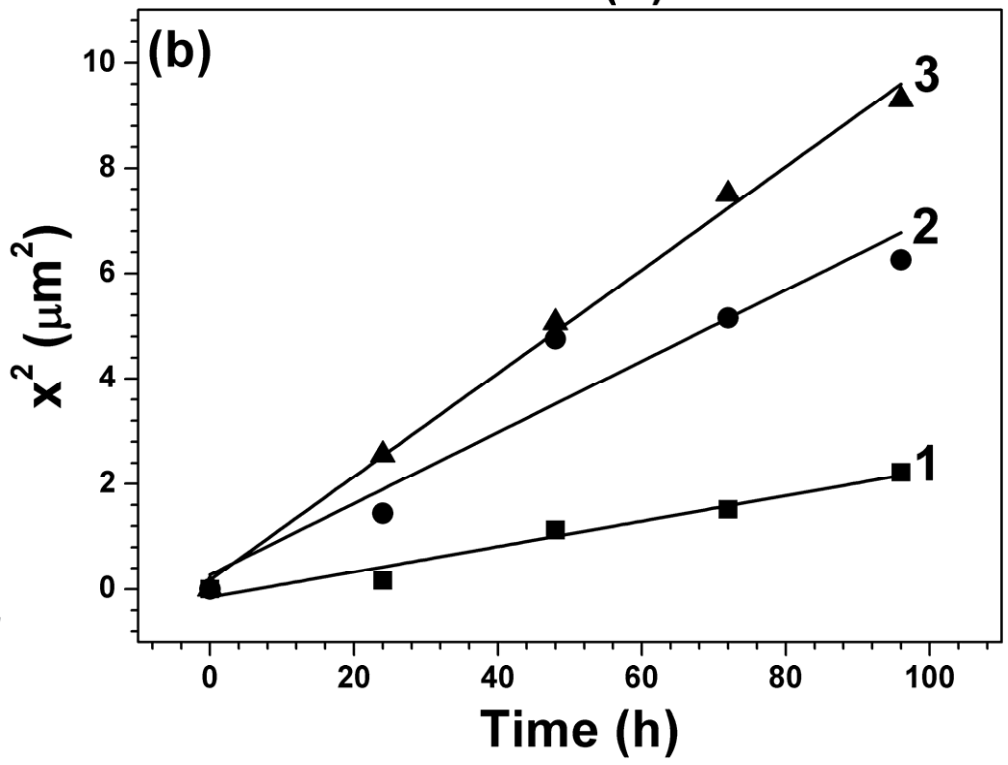
(b)
x^2 (μm^2)
Time (h)
1
2
3

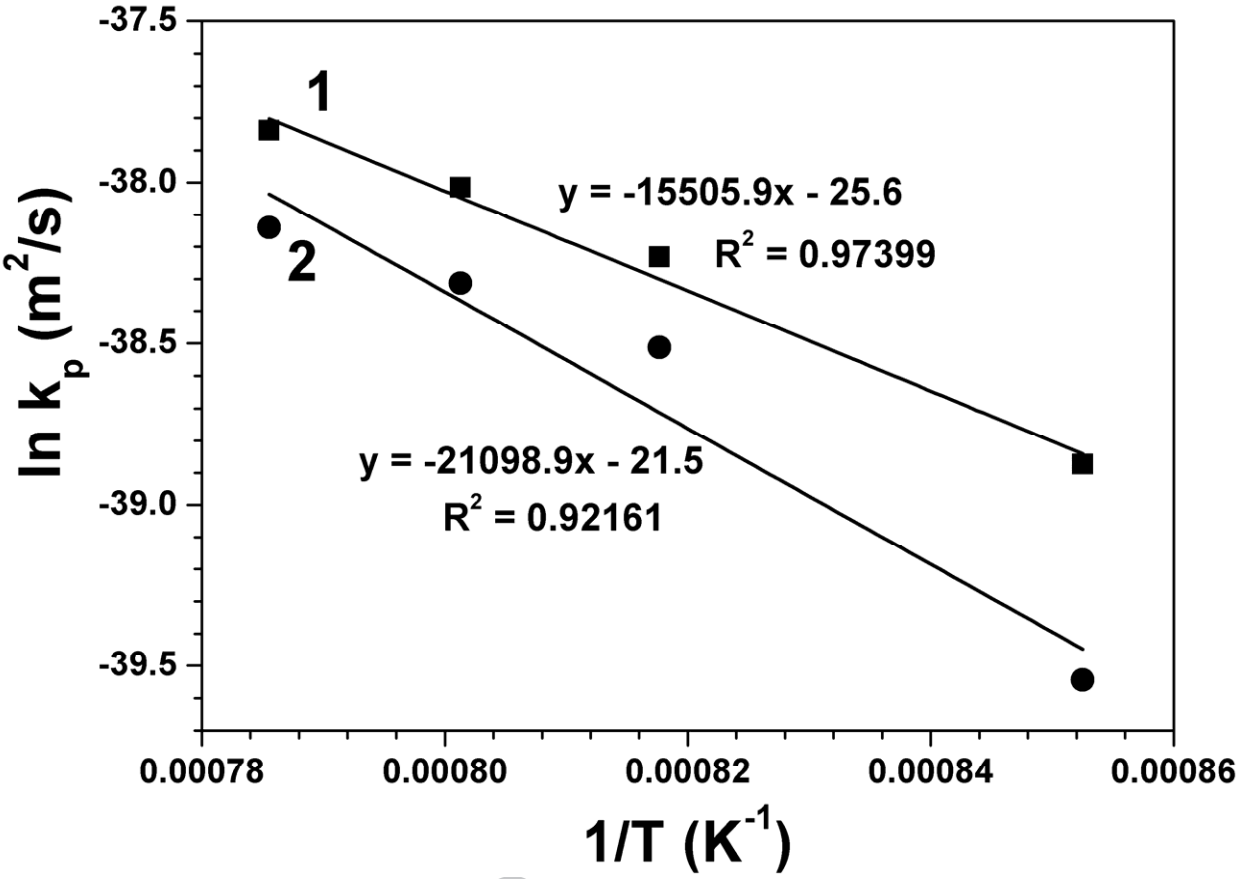
-37.5
-38.0
-38.5
-39.0
-39.5
ln k_p (m^2/s)
1
2
y = -15505.9x - 25.6
R^2 = 0.97399
y = -21098.9x - 21.5
R^2 = 0.92161
0.00078
0.00080
0.00082
0.00084
0.00086
1/T (K^-1)

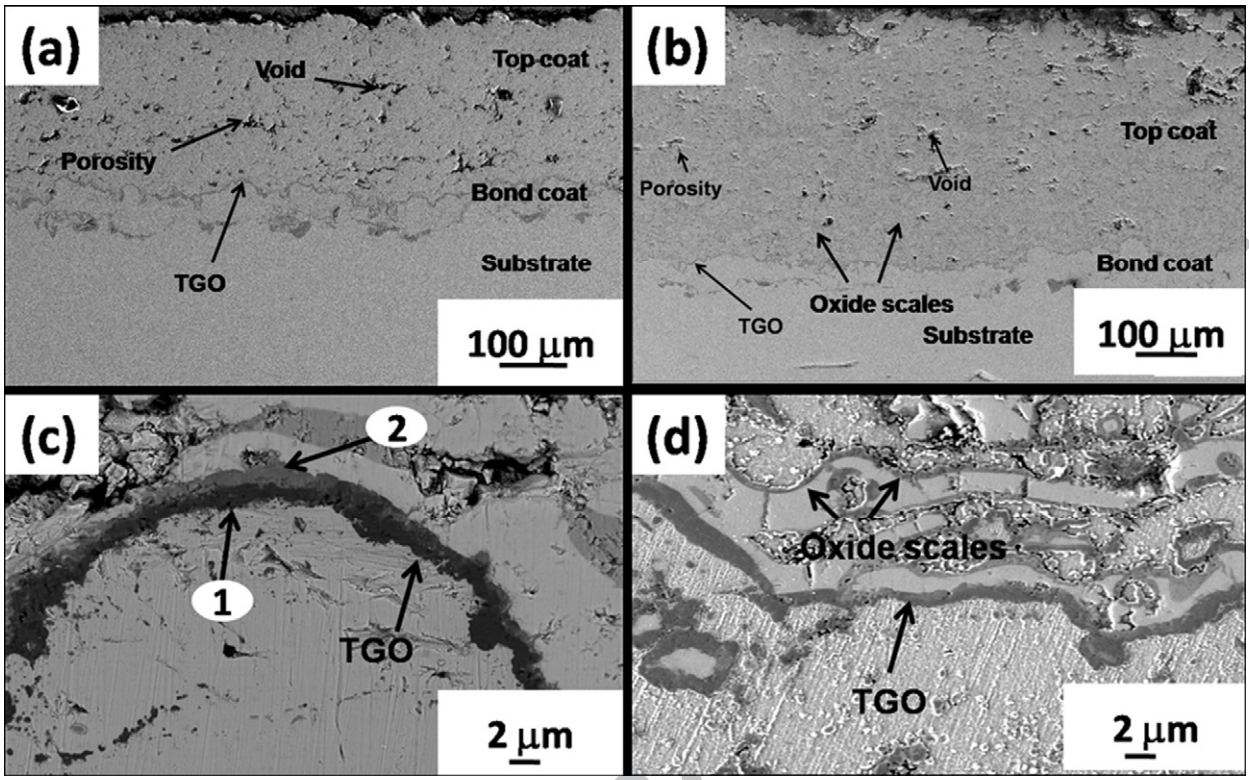

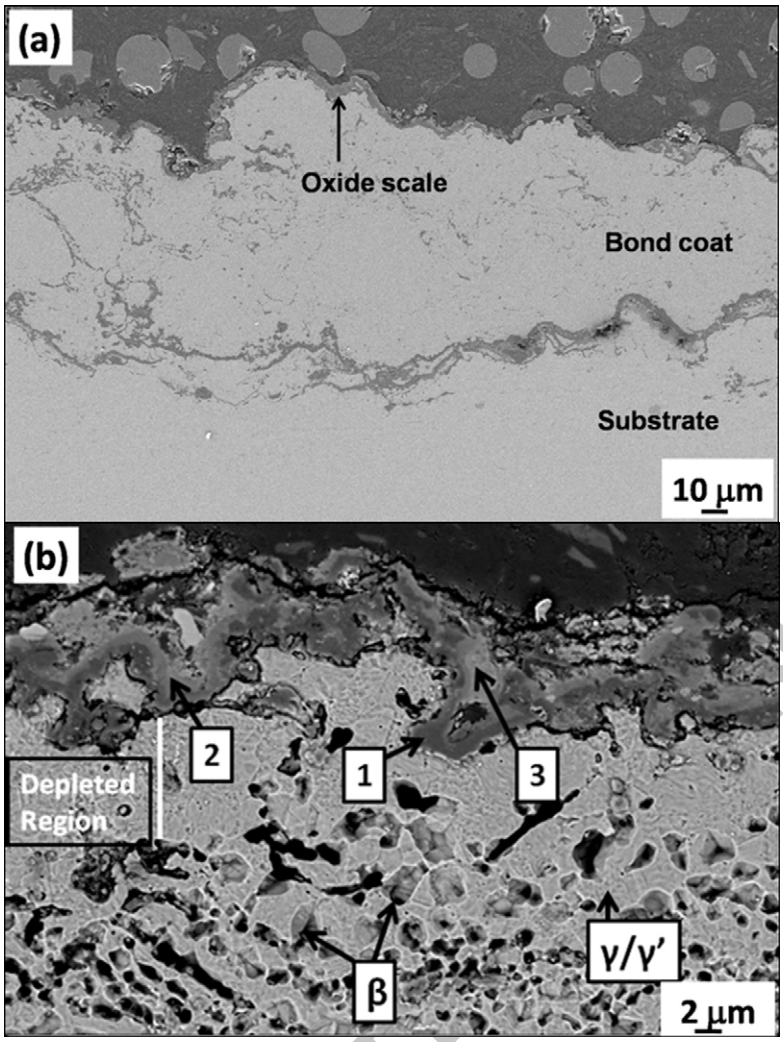

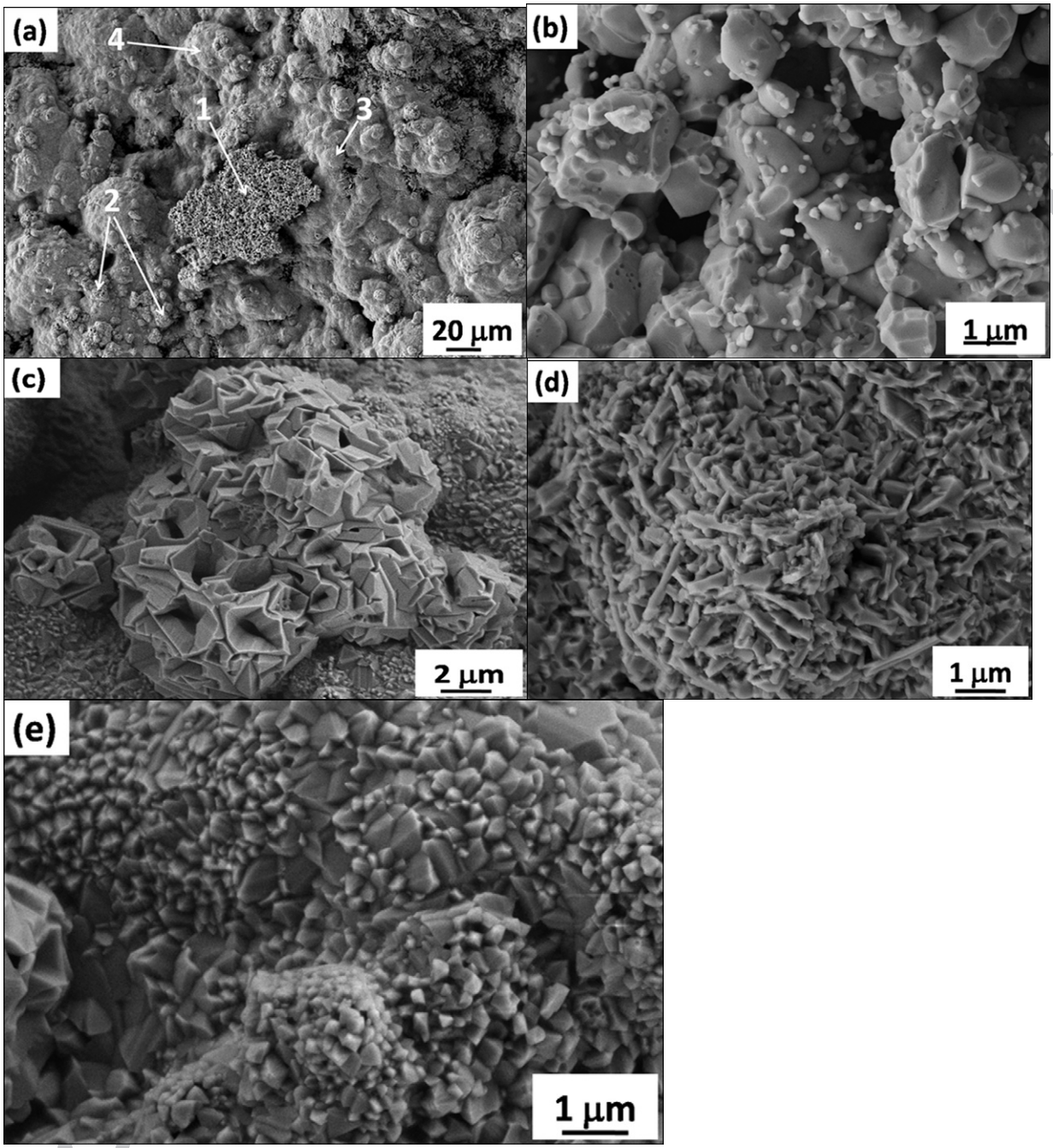
(a)
4
1
3
2
20 μm
(b)
1 μm
(c)
2 μm
(d)
1 μm
(e)
1 μm

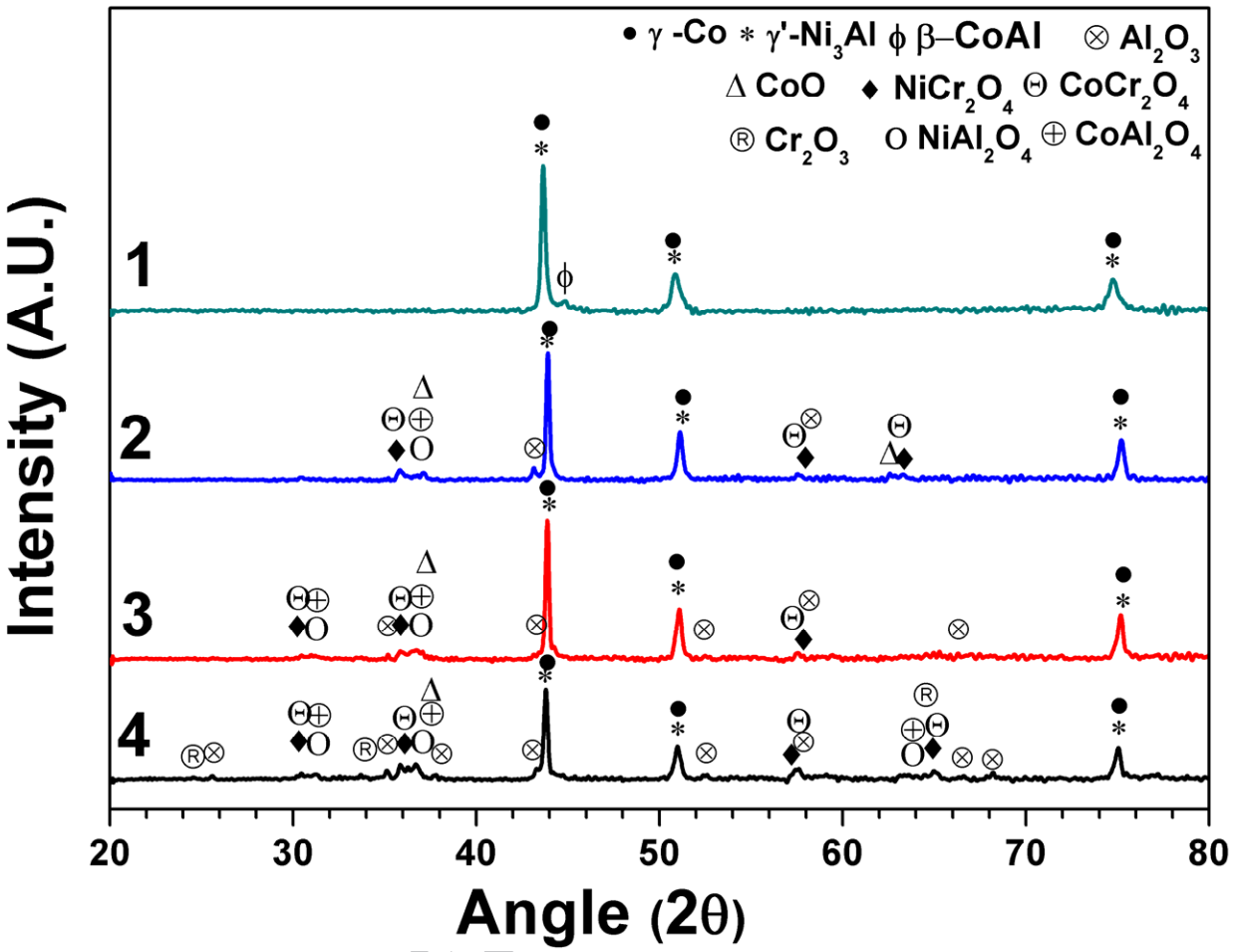
• γ -Co * γ'-Ni3Al ϕ β–CoAl ⊗ Al2O3
Δ CoO ♦ NiCr2O4 Θ CoCr2O4
® Cr2O3 O NiAl2O4 ⊕ CoAl2O4
1
2
3
4
Intensity (A.U.)
20
30
40
50
60
70
80
Angle (2θ)

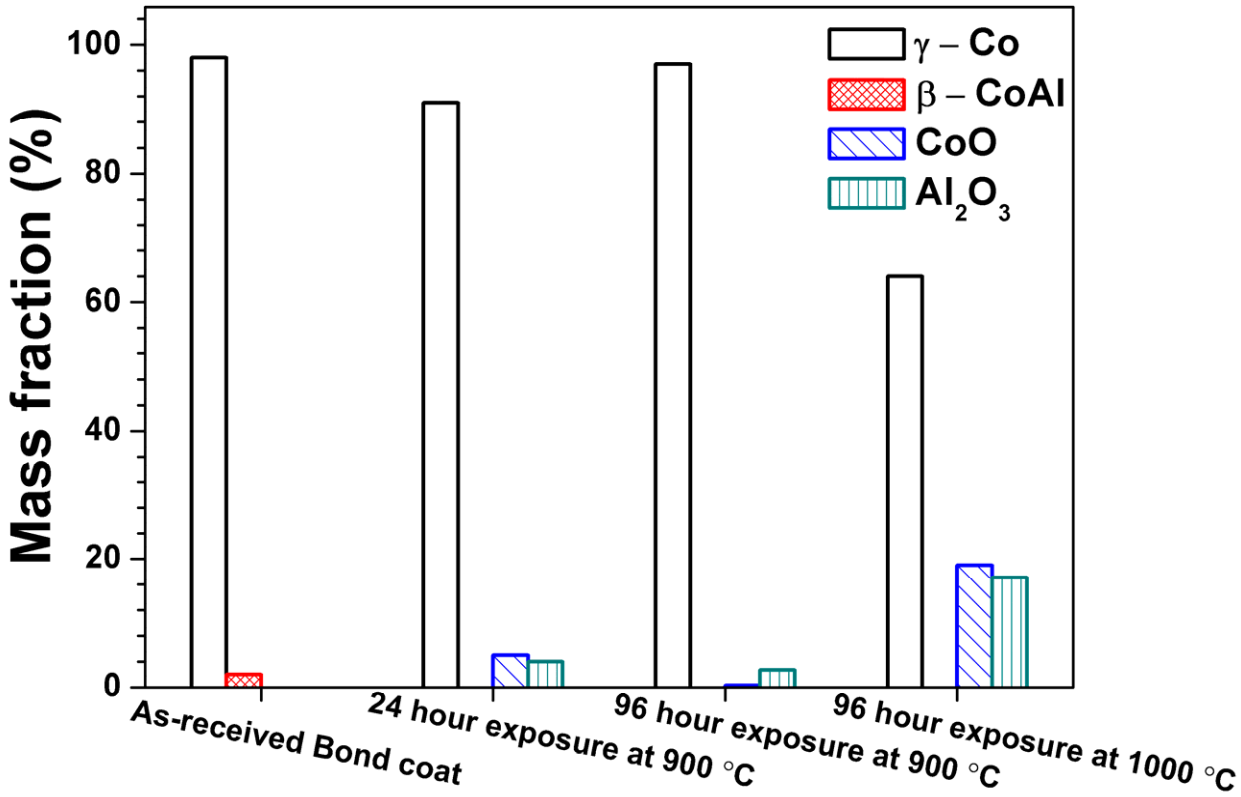

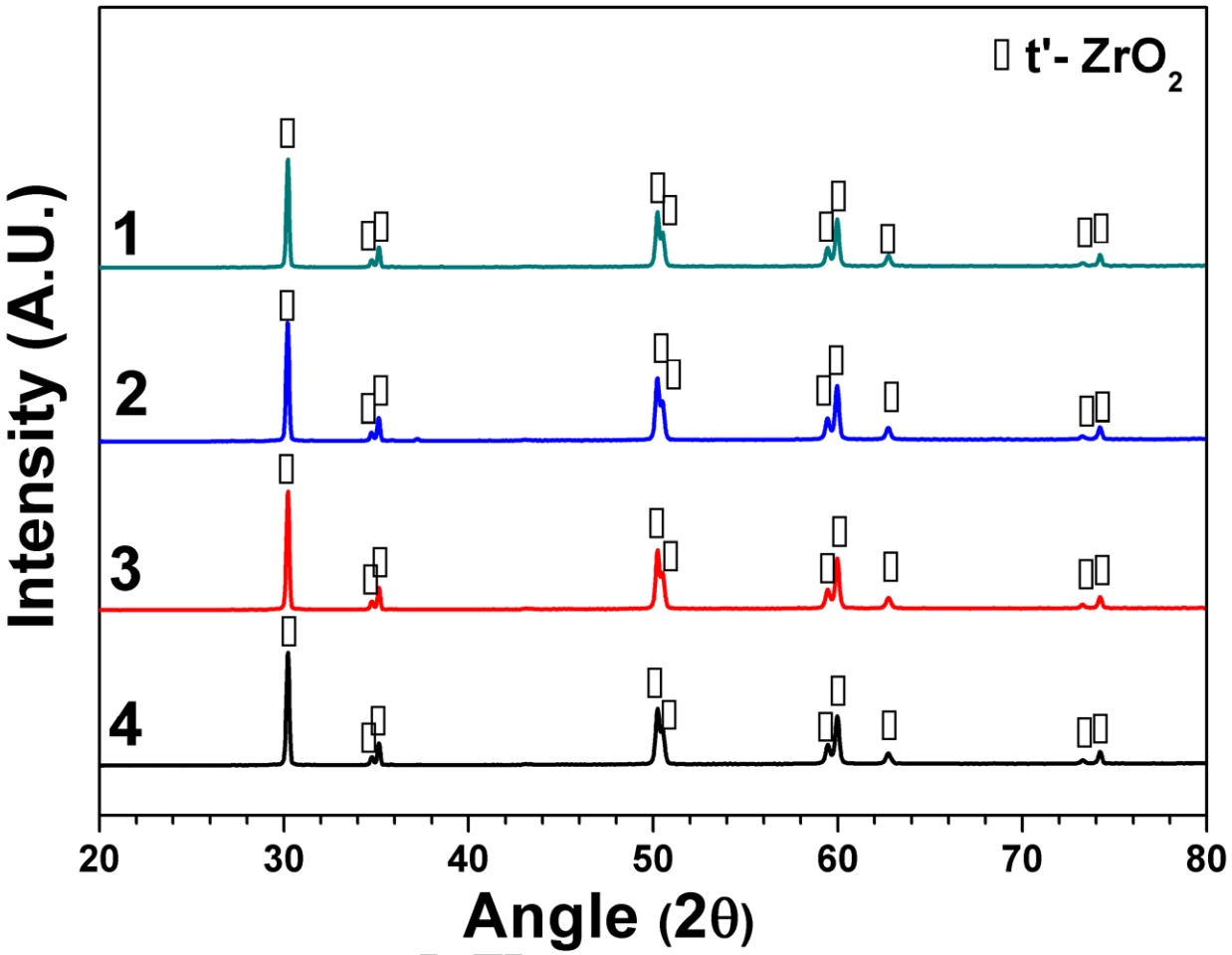

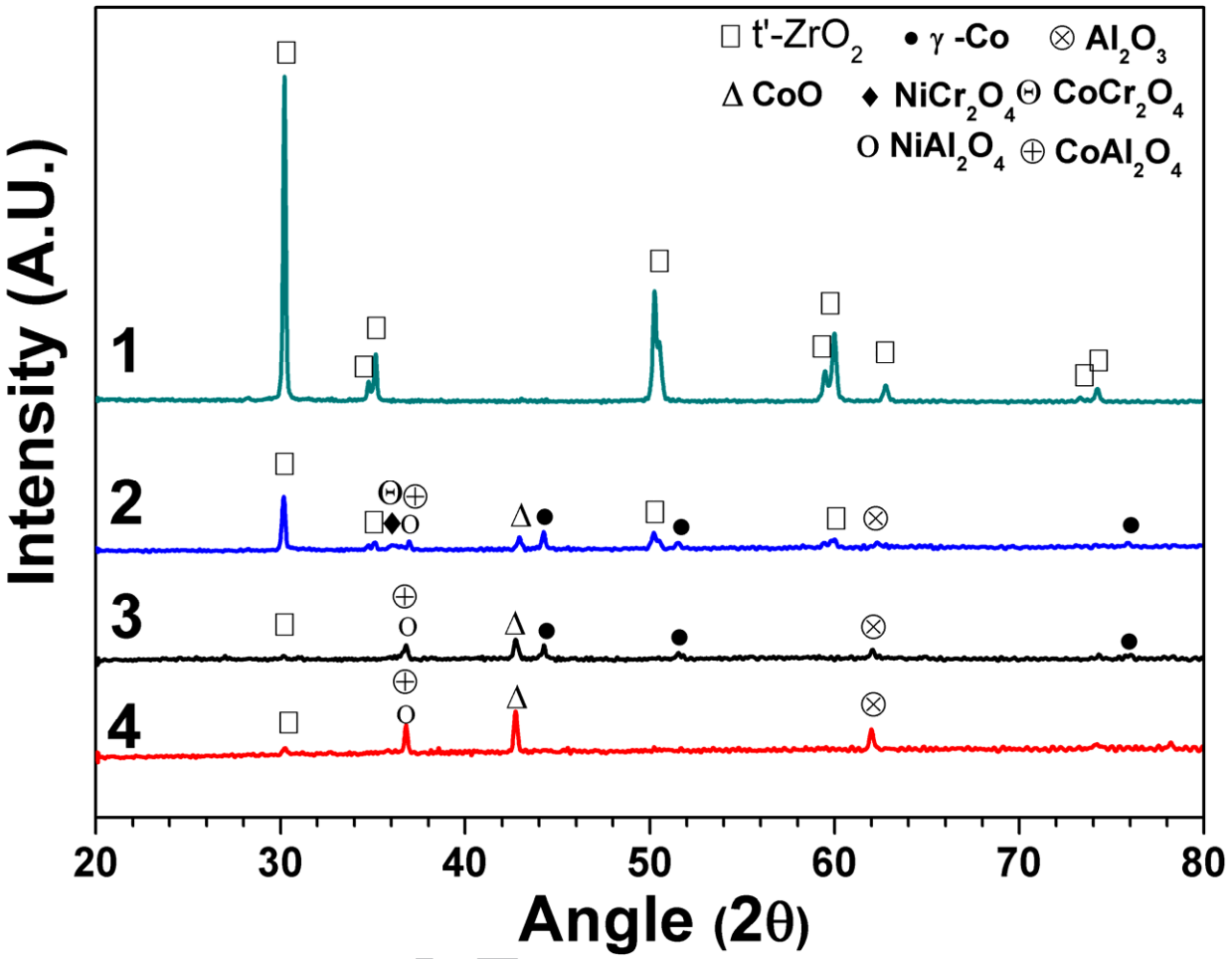
□ t'-ZrO2 • γ -Co ⊗ Al2O3
Δ CoO ♦ NiCr2O4 Θ CoCr2O4
O NiAl2O4 ⊕ CoAl2O4
Intensity (A.U.)
1
2
3
4
20
30
40
50
60
70
80
Angle (2θ)

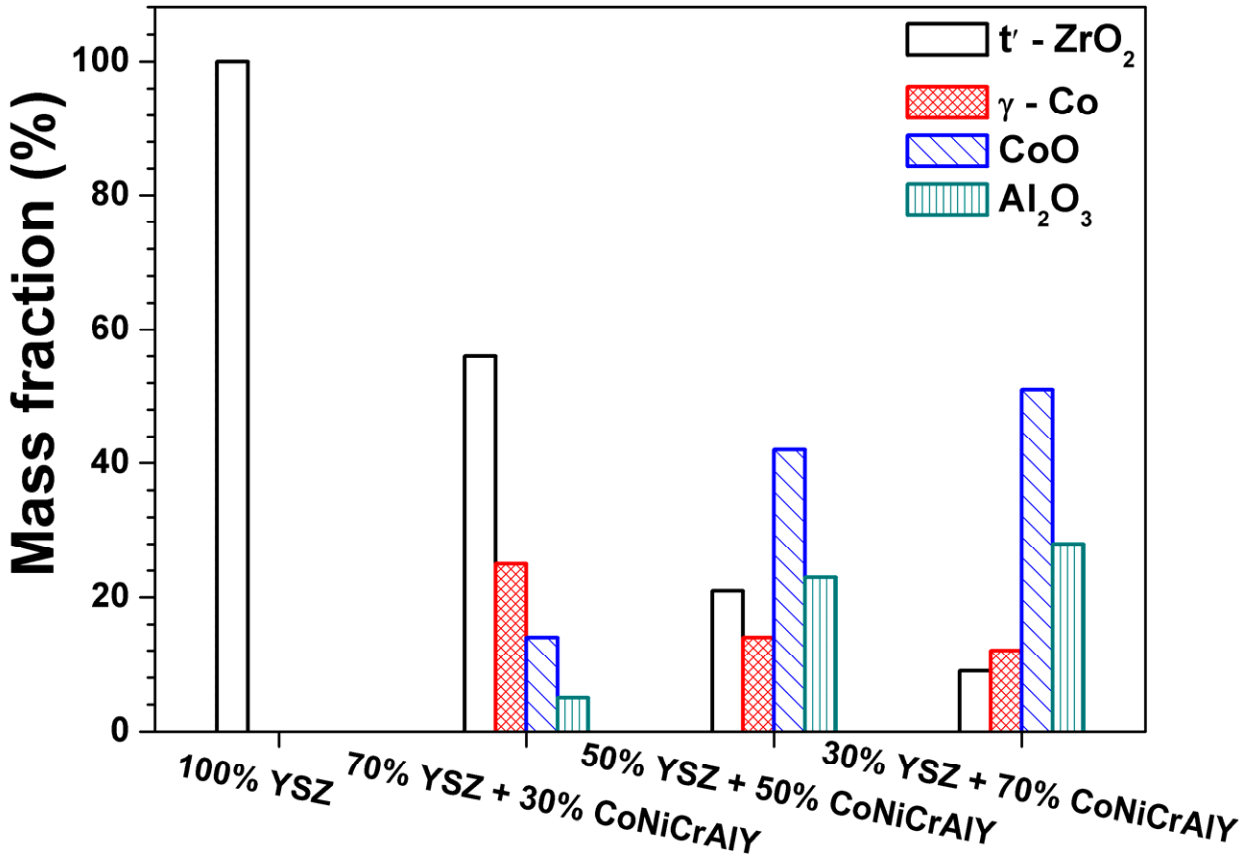
Mass fraction (%)
0
20
40
60
80
100
t′ - ZrO2
γ - Co
CoO
Al2O3
100% YSZ
70% YSZ + 30% CoNiCrAlY
50% YSZ + 50% CoNiCrAlY
30% YSZ + 70% CoNiCrAlY

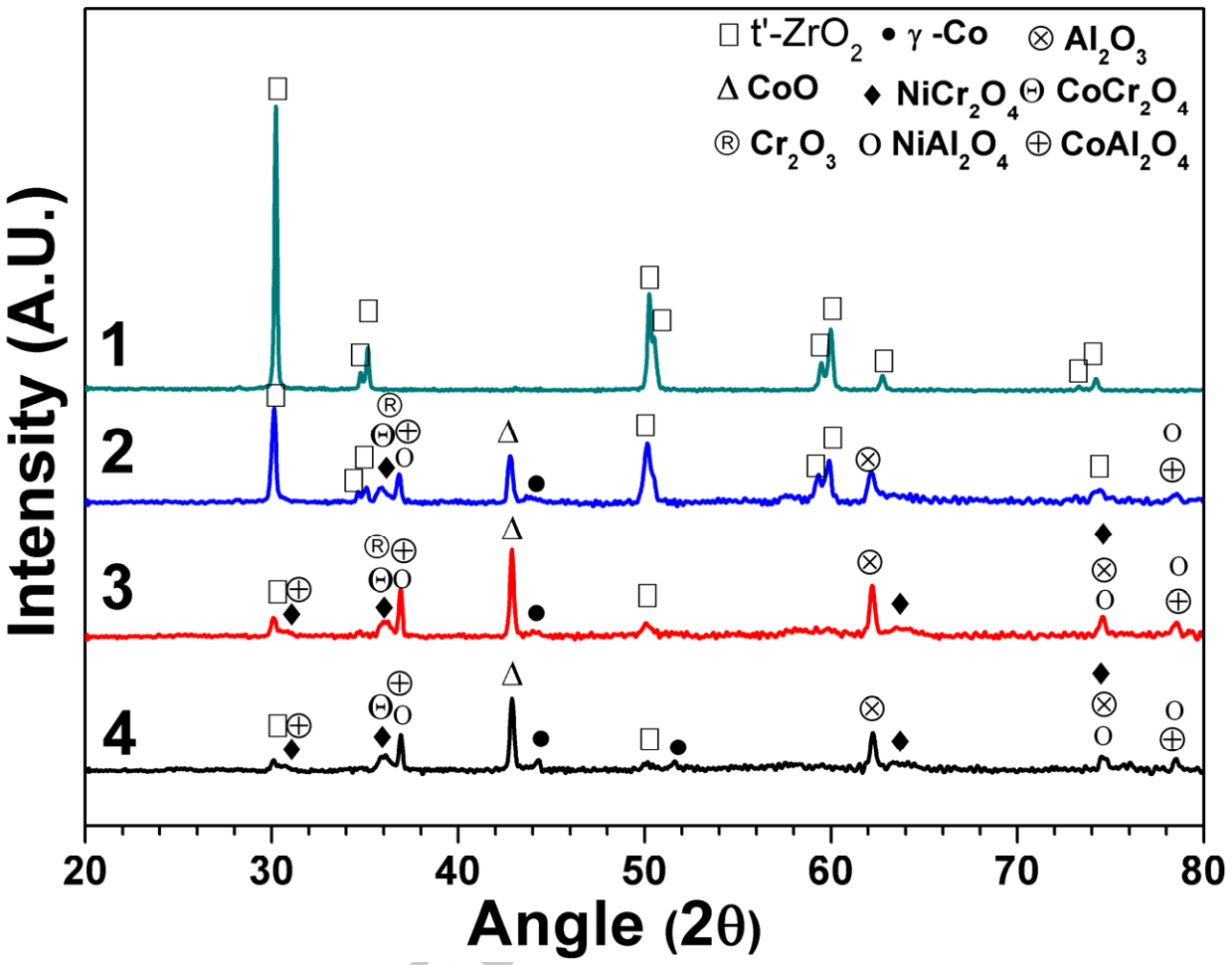
□ t'-ZrO2 • γ -Co ⊗ Al2O3
Δ CoO ♦ NiCr2O4 Θ CoCr2O4
® Cr2O3 O NiAl2O4 ⊕ CoAl2O4
Intensity (A.U.)
1
2
3
4
20
30
40
50
60
70
80
Angle (2θ)

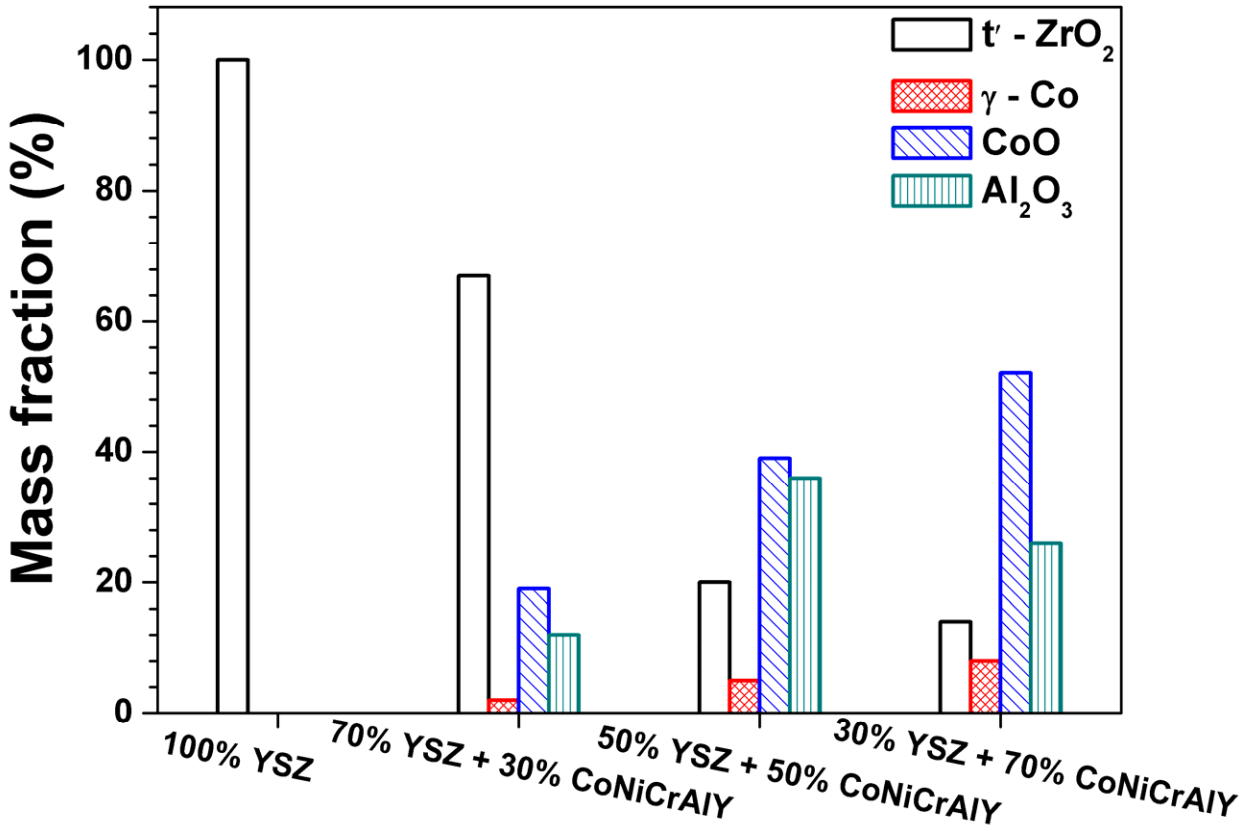

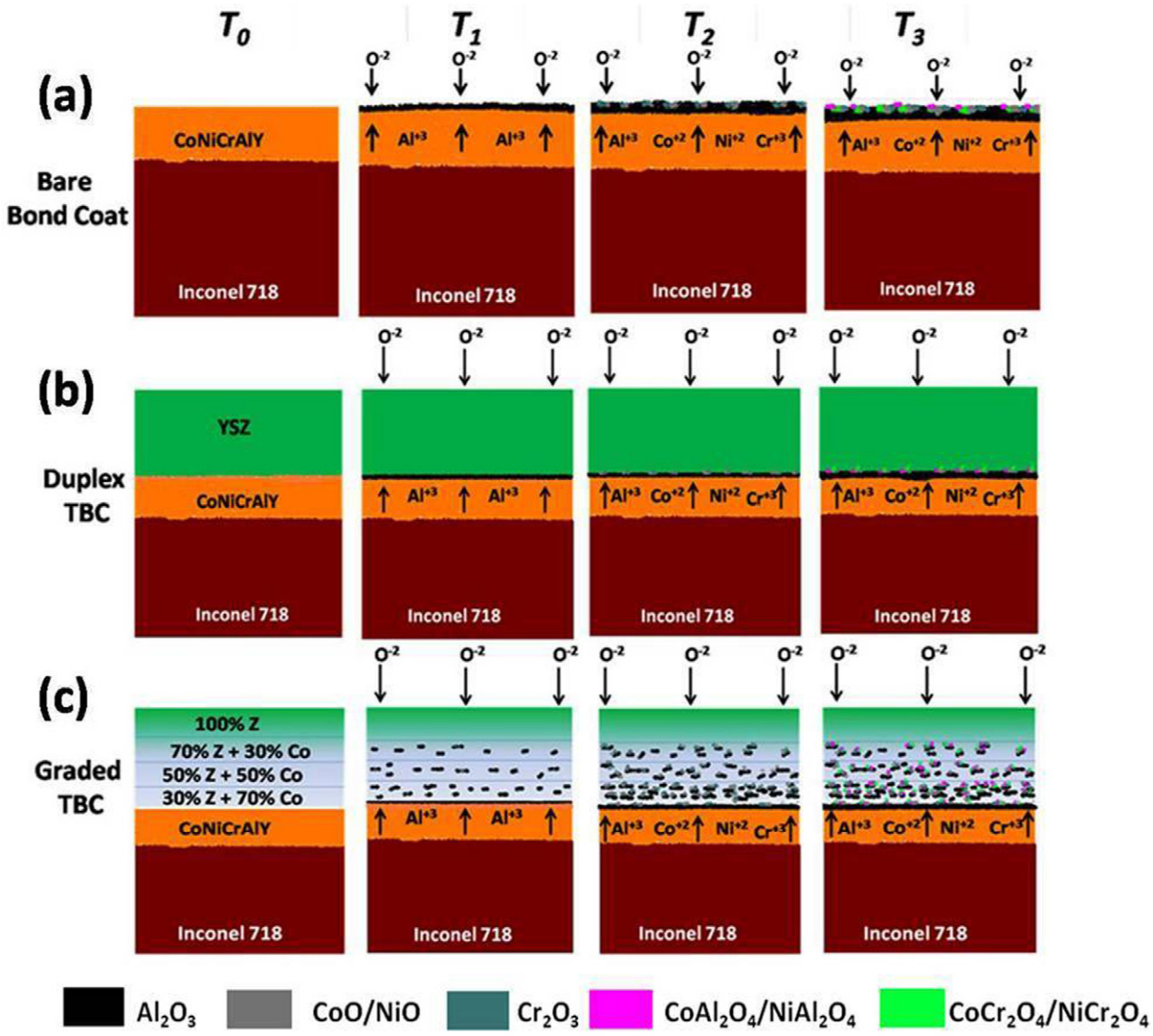

where Z: YSZ and Co: CoNiCrAlY and $T_0 < T_1 < T_2 < T_3$

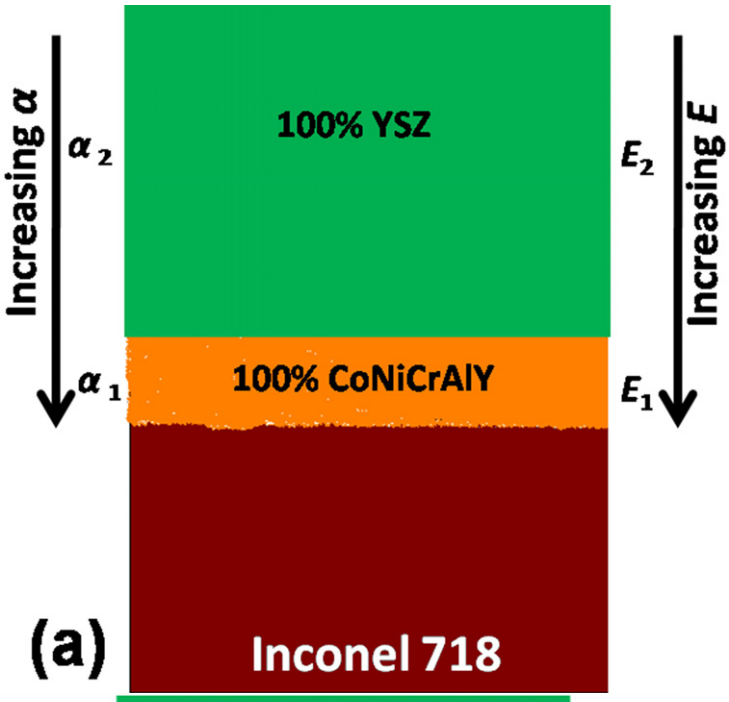

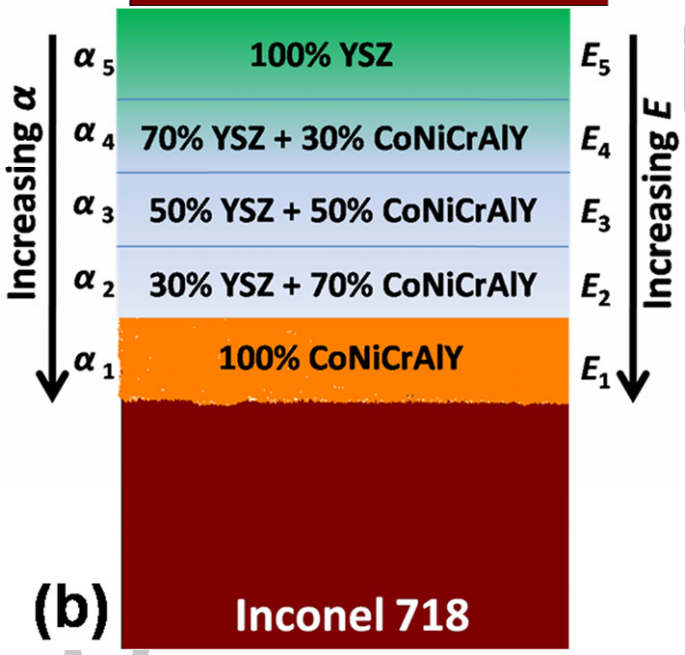

Table 1. EDS compositional analysis (atomic %) of different zones observed in Fig. 2.

	Zr	Y	Co	Ni	Cr	Al	O
A	30-32	4.12-4.35	-	-	-	-	61.23-63.02
B	-	-	38.01-38.5	31.8-32.59	17.89-18	8.25-8.47	2.1-2.68
C	-	-	0.53-1.23	0.35-0.88	3.20-4.62	34.10-35.88	54.38-58.07
D	-	-	10.08-16.36	4.46-10.92	9.65-10.68	11.55-17.15	51.52-58.63

Table 2. Rate constant and activation energy values for duplex and compositionally graded thermal barrier coating system.

System	Rate constant, k_p (m^2/s)				Activation energy (kJ/mol)	R^2	Literature Activation energy (kJ/mol)
	900 °C	950 °C	975 °C	1000 °C			
Duplex TBC	1.31×10^{-17}	2.49×10^{-17}	3.09×10^{-17}	3.69×10^{-17}	129	0.97	212 (non-isothermal oxidation) [30], 139 [41], 188 [42], 130 [43], 102 [44]
Graded TBC	0.67×10^{-17}	1.88×10^{-17}	2.29×10^{-17}	2.73×10^{-17}	175	0.92	419 (non-isothermal oxidation) [30]

Table 3. EDS compositional analysis (atomic %) of oxides scales formed on the cross-section of bare bond coat oxidized at 1000°C for 96 hours as shown in Fig. 7b.

	Co	Ni	Cr	Al	O
1	1.6-3.37	1.55-3.83	2.6-6.88	36.87-38.57	49.06-55.68
2	6.89-8.04	3.05-3.72	16.53-18.92	14.07-16.95	54.19-57.63
3	3.55-5.07	3.27-4.14	17.73-20.23	7.4-8.12	56.09-60.04

Table 4. EDS compositional analysis (atomic %) of different oxides formed on top of bare bond coat oxidized at 1000 °C for 96 hours as shown in Fig. 8a.

	Co	Ni	Cr	Al	O
1	-	-	30.81-37.82	-	61.09-68.17
2	14.02-16.27	2.35-4.34	12.25-19.94	1.01-2.86	60.89-63.96
3	2.82-5.45	2.24-5.43	1.9-3.11	27.01-27.84	59.38-65.10
4	12.3-18.94	11.36-17.97	6.81-9.86	1.75-2.05	64.27-66.58

Table 5. Standard Gibb's free energy of formation and thermodynamic activity of elements present in the bond coat alloy to form their respective oxides at $P_{O2} = 1$ atm [47].

Phase	Standard free energy of formation, $\Delta G°$ (kJ/mol)		Equilibrium constant, K_i		Thermodyna-micactivity of oxides, a_i	Elements	Thermodynamic activity of elements, a_i	
	1173 K	1273 K	1173 K	1273 K			1173 K	1273 K
Al_2O_3	- 1618.3	- 1613.1	1.17×10^{72}	1.56×10^{66}	1	Al	9.25×10^{-37}	8.03×10^{-34}
Cr_2O_3	- 1035.2	- 1027	1.26×10^{46}	1.39×10^{42}	1	Cr	8.86×10^{-24}	8.47×10^{-22}
CoO	- 176.9	- 171.7	0.75×10^{8}	1.1×10^{7}	1	Co	1.15×10^{-4}	3.01×10^{-4}
NiO	- 196	- 192.2	0.54×10^{9}	0.77×10^{8}	1	Ni	4.32×10^{-5}	1.14×10^{-4}
$CoAl_2O_4$	- 83.3	- 93.3	-	-	-	-	-	-
$NiAl_2O_4$	- 109.3	- 115.42	-	-	-	-	-	-
$CoCr_2O_4$	- 88.8	- 101.5	-	-	-	-	-	-
$NiCr_2O_4$	132.2	158	-	-	-	-	-	-

Table 6. Residual stress after isothermal oxidation at 900°C in compositionally graded TBC.

Sample	Residual stress (MPa)					
	As-sprayed		24 hour		72 hour	
	σ_{11}	σ_{22}	σ_{11}	σ_{22}	σ_{11}	σ_{22}
100% YSZ	73.1	17.2	37	15.9	103	102.1
70% YSZ+30% CoNiCrAlY	-28 .7	45.9	-107	87.5	-139.5	144.1
50% YSZ+50% CoNiCrAlY	-90	47.1	-101.3	-65.7	-298	56.5
30% YSZ+70% CoNiCrAlY	-171.6	142.3	-364.7	-0.5	-516.4	452.9
100% CoNiCrAlY	-274.1	-62.5	-1787	-1388.7	-1601.9	-1459.9

Table 7. Residual stress after isothermal oxidation at 1000°C in compositionally graded TBC.

Sample	Residual stress (MPa)					
	As-sprayed		24 hour		72 hour	
	σ_{11}	σ_{22}	σ_{11}	σ_{22}	σ_{11}	σ_{22}
100% YSZ	73.1	17.2	172.3	93.4	164.1	144.5
70% YSZ+30% CoNiCrAlY	-28 .7	45.9	-31.7	-111.4	- 133.7	225.4
50% YSZ+50% CoNiCrAlY	-90	47.1	-373.8	-261	-442	230.3
30% YSZ+70% CoNiCrAlY	-171.6	142.3	-391.8	-492.9	-672.8	-473
100% CoNiCrAlY	-274.1	-62.5	-1530.6	-1237.5	-1582.4	-1325.3

Highlights

- Study of isothermal oxidation kinetics of YSZ based thermal barrier coating (TBC).
- Compositionally graded TBC shows lower oxidation kinetics than duplex one.
- Presence of Al_2O_3 and spinel oxides were found in the microstructure.
- Lower oxidation kinetics in graded TBC was due to reduced spinel oxides.